Seismological monitoring of landquakes and river bedload transport

透過地震方法監測地表崩塌事件與河床載搬運

Vvn Weian Chao (趙韋安)

Department of Geosciences, National Taiwan University

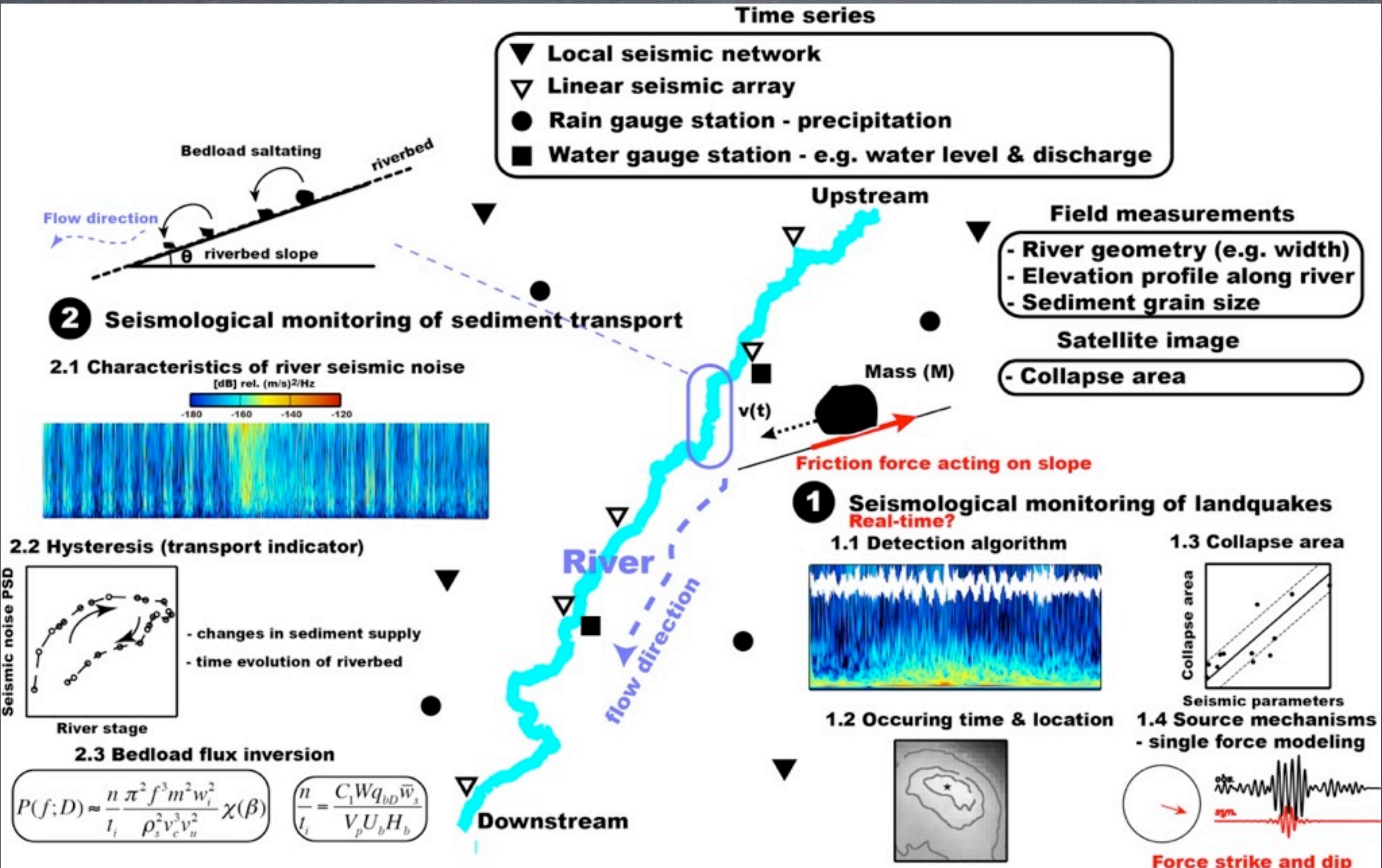
Time series
Local seismic network
Linear seismic array
Rain gauge station - precipitation
Water gauge station - e.g. water level & discharge
Bedload saltating
riverbed
Flow direction
θ riverbed slope
Upstream
Field measurements
- River geometry (e.g. width)
- Elevation profile along river
- Sediment grain size
Satellite image
- Collapse area
2 Seismological monitoring of sediment transport
2.1 Characteristics of river seismic noise
[dB] rel. (m/s)²/Hz
-180 -160 -140 -120
Mass (M)
v(t)
Friction force acting on slope
1 Seismological monitoring of landquakes
Real-time?
1.1 Detection algorithm
1.3 Collapse area
2.2 Hysteresis (transport indicator)
River
flow direction
Seismic noise PSD
- changes in sediment supply
- time evolution of riverbed
River stage
Collapse area
Seismic parameters
1.2 Occuring time & location
1.4 Source mechanisms
- single force modeling
2.3 Bedload flux inversion
$P(f;D) \approx \frac{n}{t_i}\frac{\pi^2 f^3 m^2 w_i^2}{\rho_s^2 v_c^3 v_u^2}\chi(\beta)$
$\frac{n}{t_i} = \frac{C_1 W q_{bD} \overline{w}_s}{V_p U_b H_b}$
Downstream
obs.
syn.
Force strike and dip

A seismological study of landquake from real-time broadband seismic networks

Geophys. J. Int. (2013) doi: 10.1093/gji/ggt121
Geophysical Journal International Advance Access published April 29, 2013

A seismological study of landquakes using a real-time broad-band seismic network

Chi-Hsuan Chen,[1,3] Wei-An Chao,[1] Yih-Min Wu,[1] Li Zhao,[2] Yue-Gau Chen,[1] Wan-Yun Ho,[1] Ting-Li Lin,[4] Kuan-Hung Kuo[5] and Jui-Ming Chang[1]

Chen et al. (2013, GJI)

Detection of spectrogram

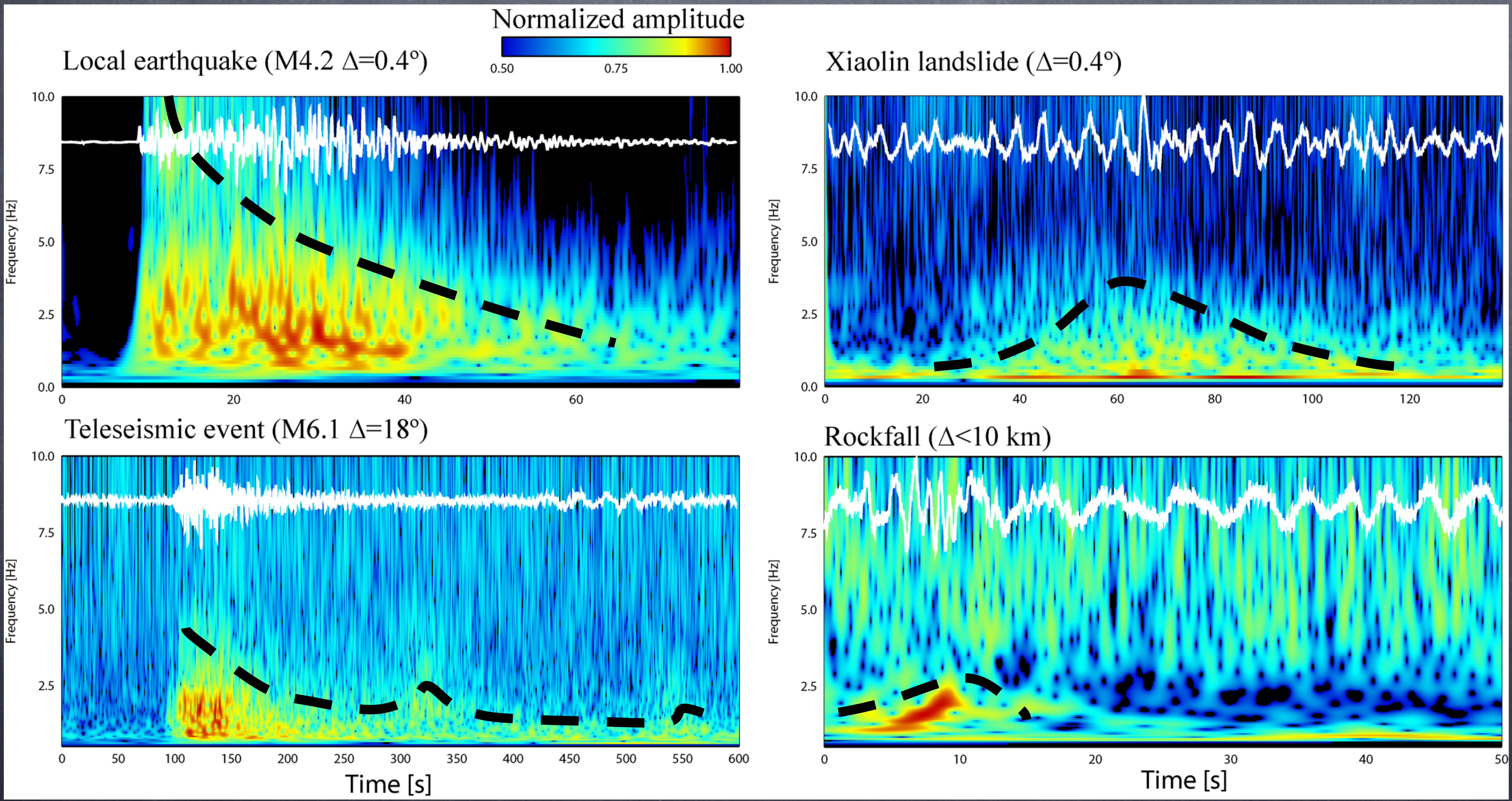

Shiaolin event

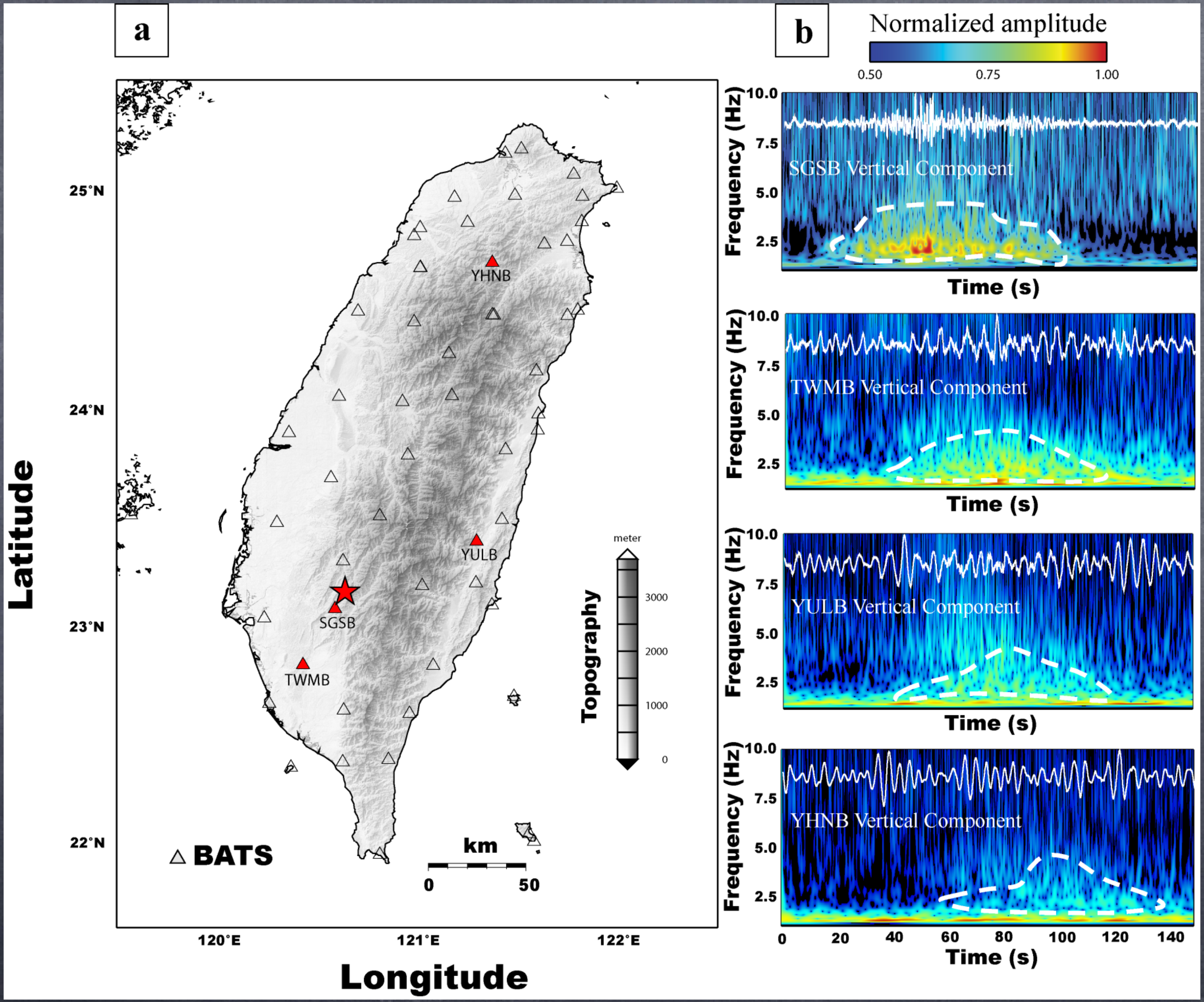

Landquake Epicenter Determination (LED)

$$A_m(\xi) = \frac{1}{N_p}\sum_{i=1}^{n}\sum_{j=i+1}^{n}(C_{ij}^{\max} - C_{ij}(\Delta T_S(\xi))) \times w_{ij}$$

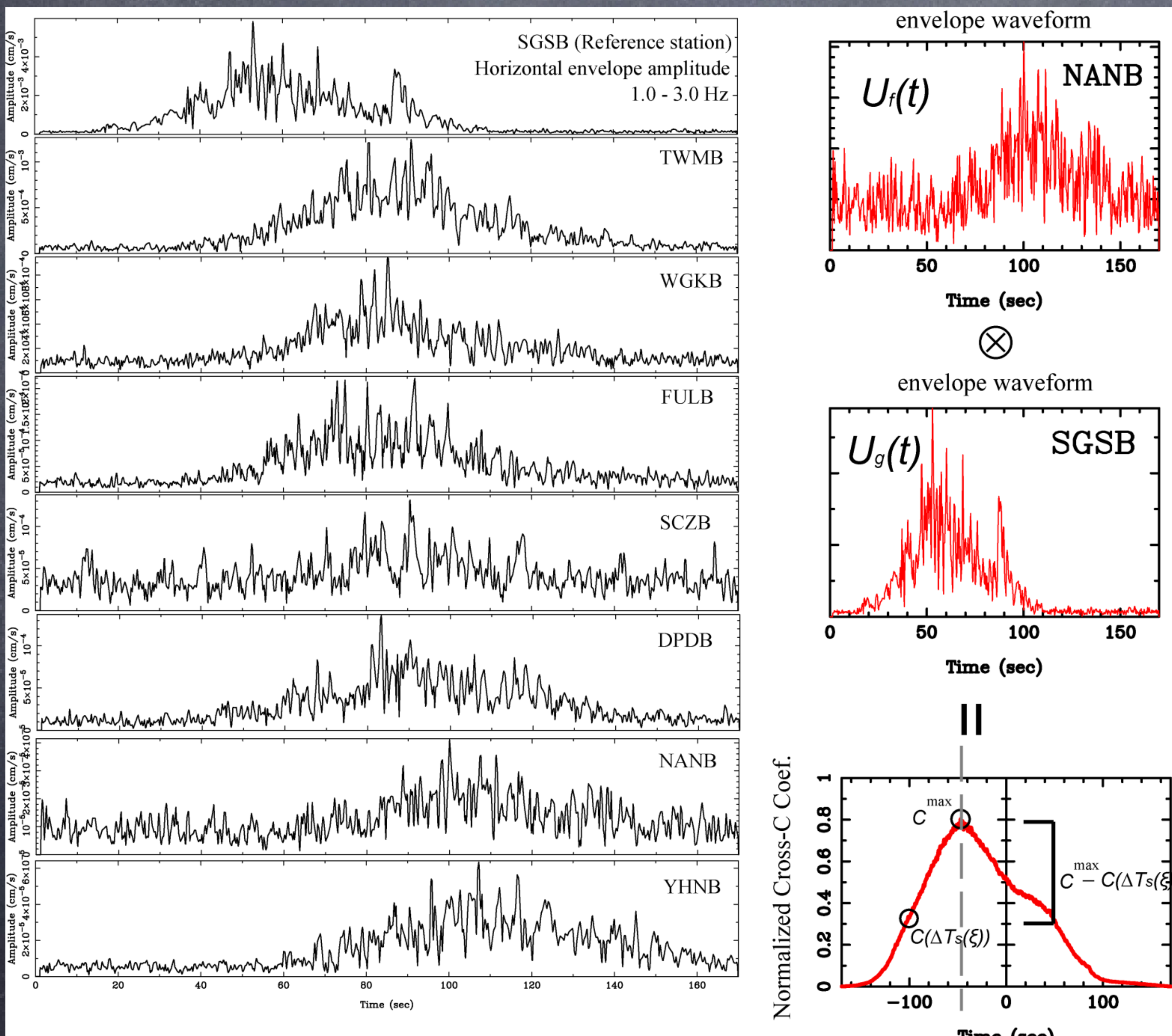

SNR > 2.5

C^{max} > 0.7

Station number ≥ 3

Fixed topography

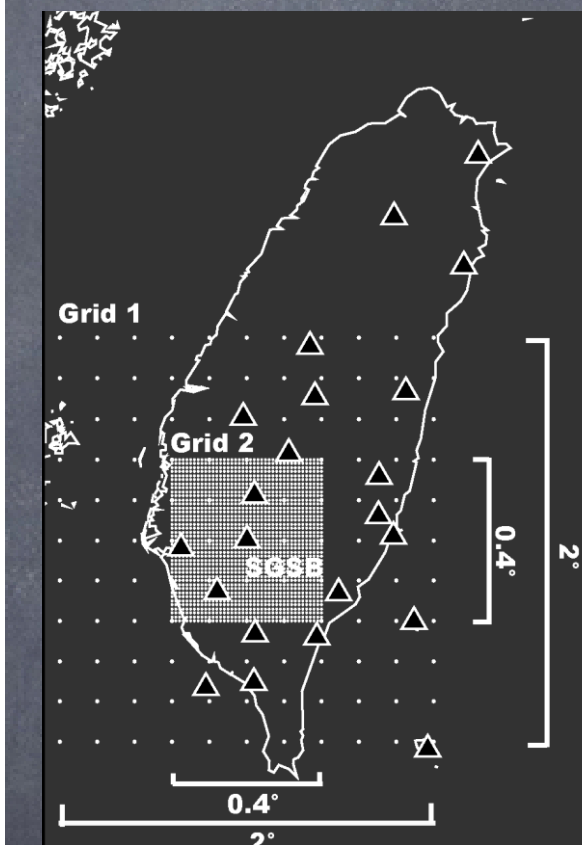

Landquake Epicenter Determination (LED)

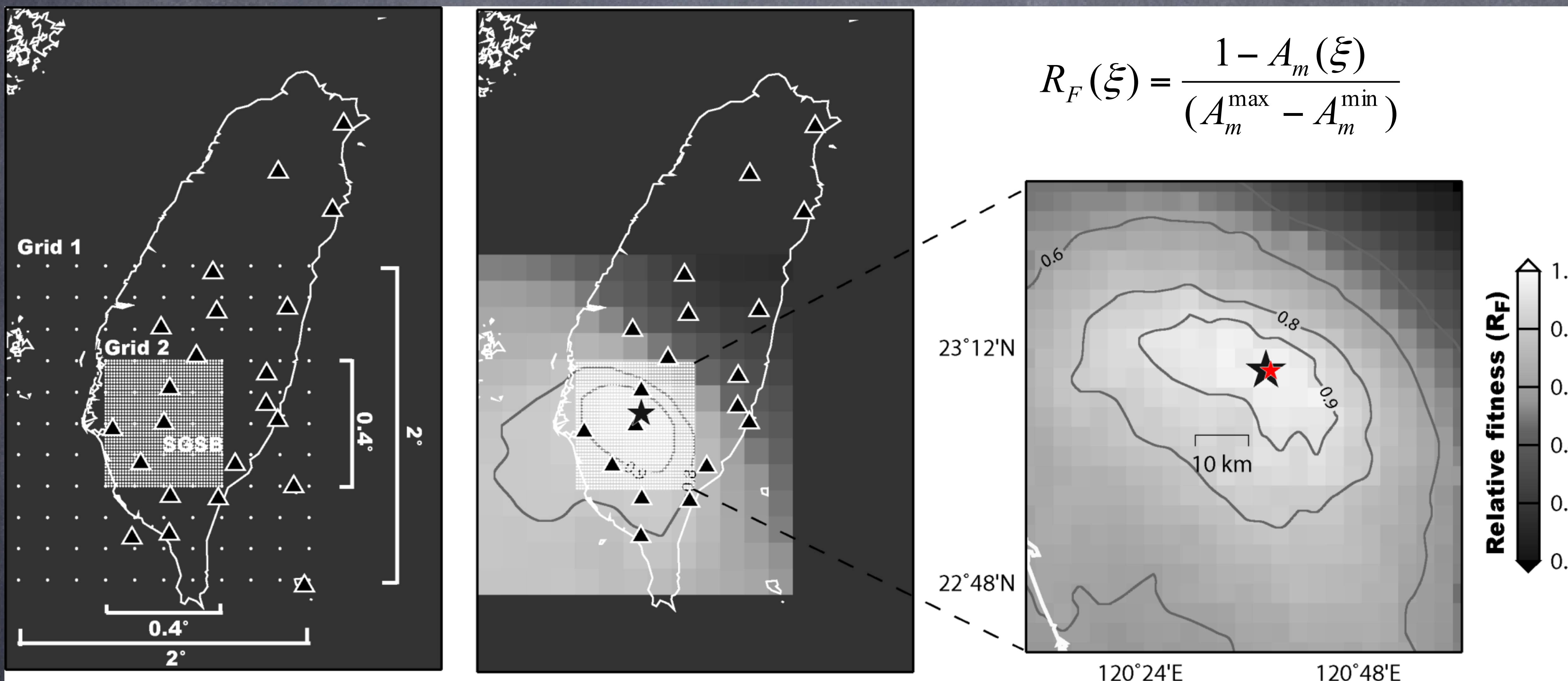

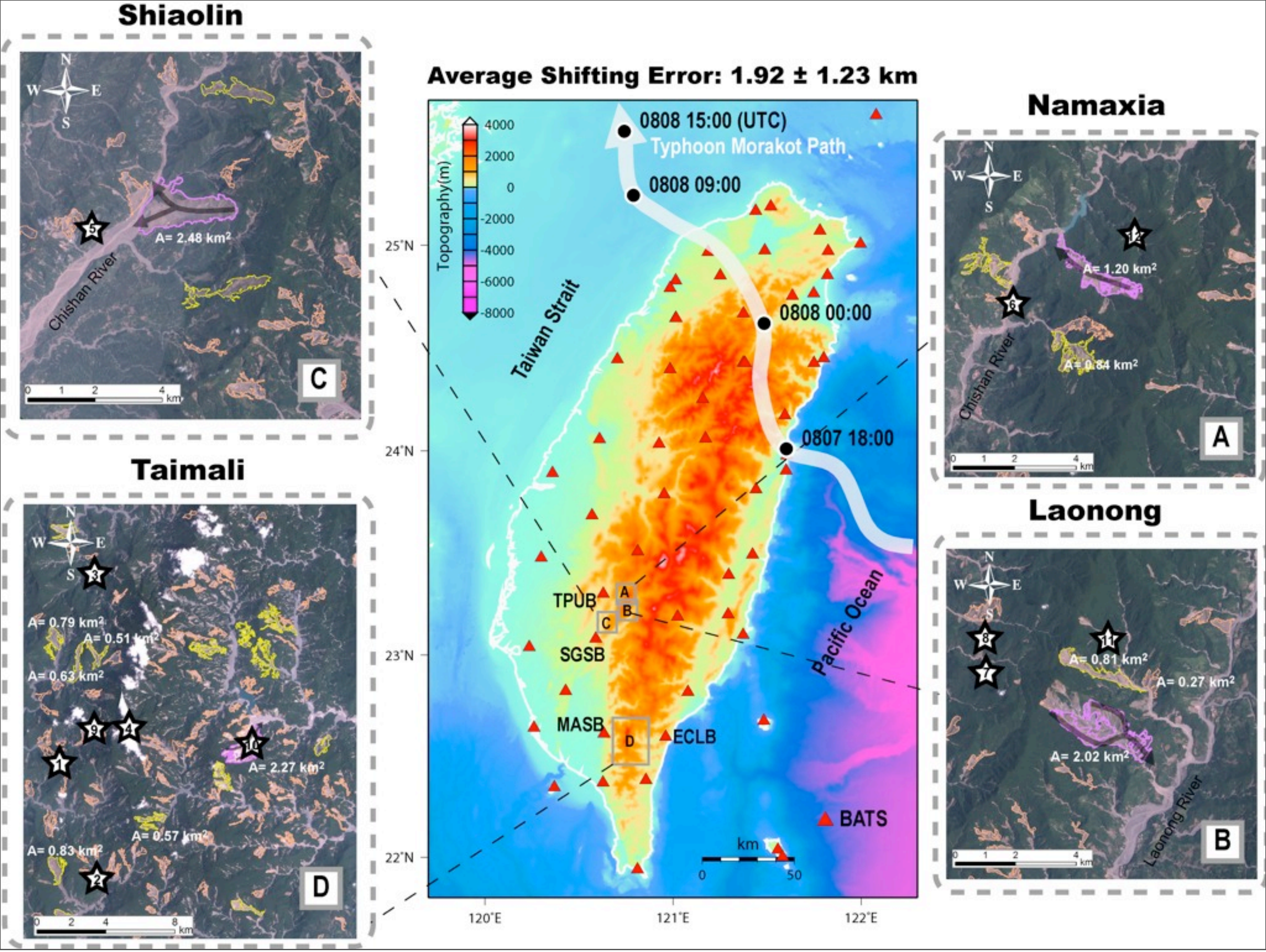
Shiaolin
A= 2.48 km2
Chishan River
C
Average Shifting Error: 1.92 ± 1.23 km
0808 15:00 (UTC)
Typhoon Morakot Path
0808 09:00
0808 00:00
0807 18:00
Topography(m)
Taiwan Strait
Pacific Ocean
TPUB
SGSB
MASB
ECLB
BATS
25°N
24°N
23°N
22°N
120°E
121°E
122°E
Namaxia
A= 1.20 km2
A= 0.84 km2
Chishan River
A
Taimali
A= 0.79 km2
A= 0.51 km2
A= 0.63 km2
A= 2.27 km2
A= 0.57 km2
A= 0.83 km2
D
Laonong
A= 0.81 km2
A= 0.27 km2
A= 2.02 km2
Laonong River
B

Seismic parameters

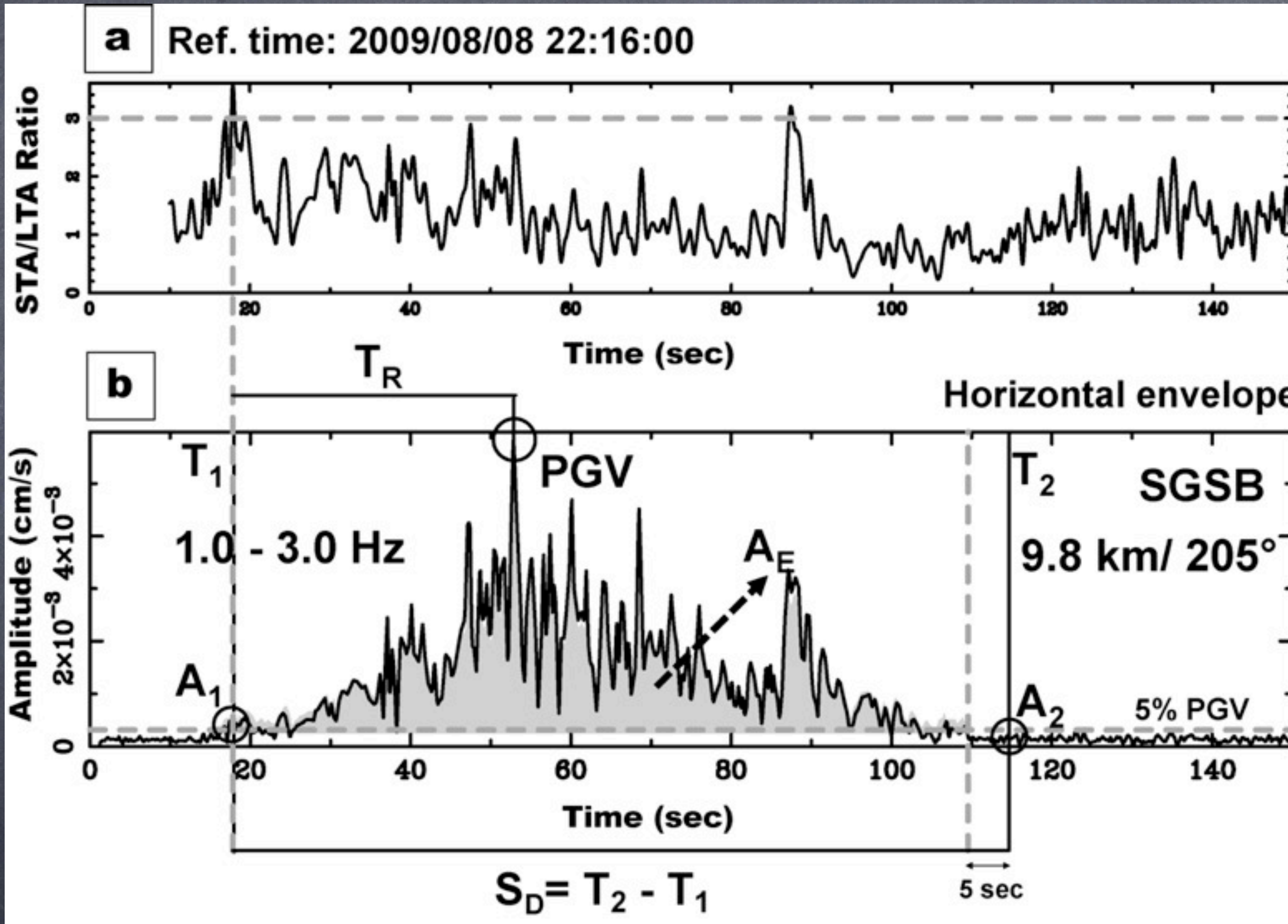

a. Scaling between envelope area and collapse

b. Limitation of detection

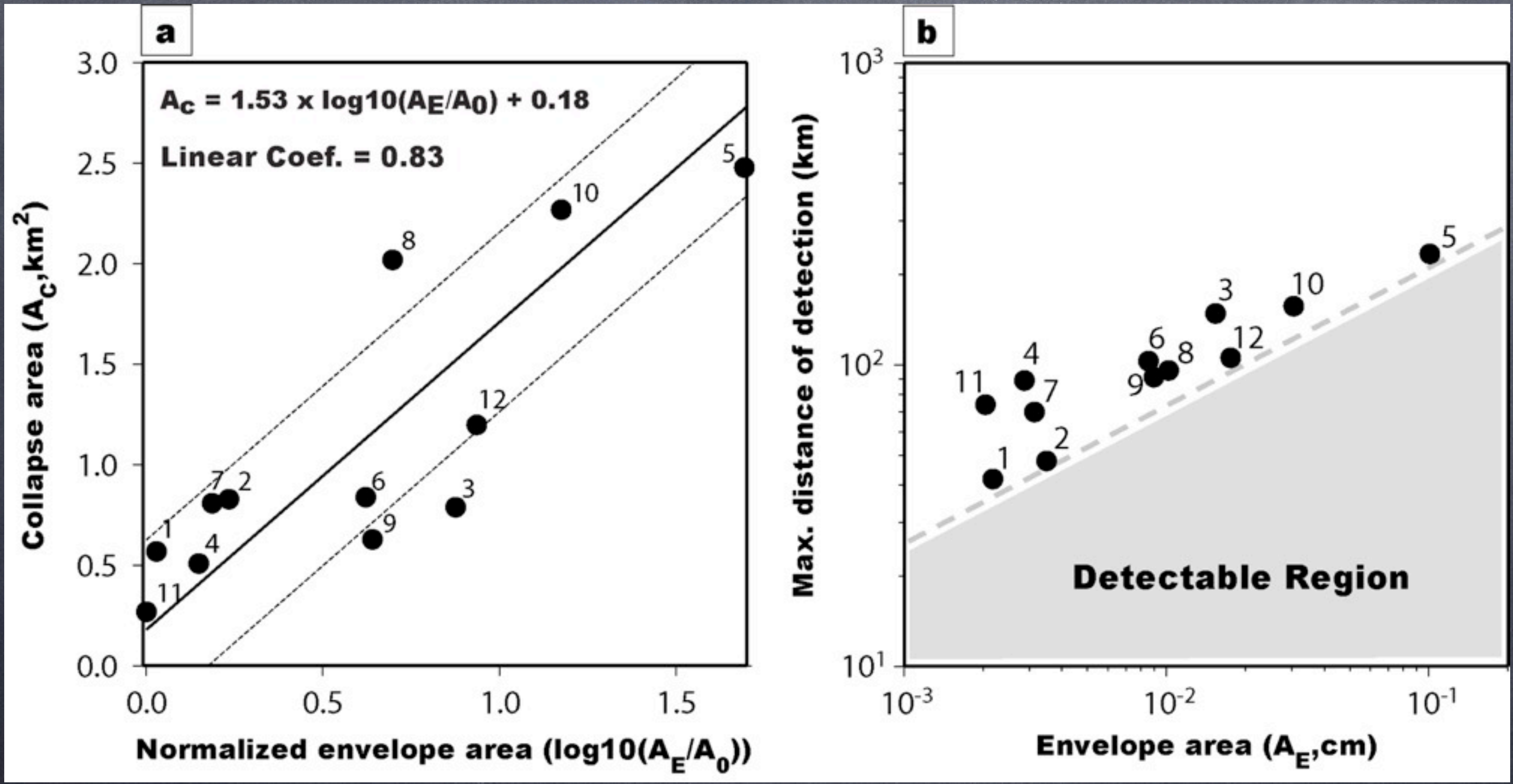

Identification of landquake type

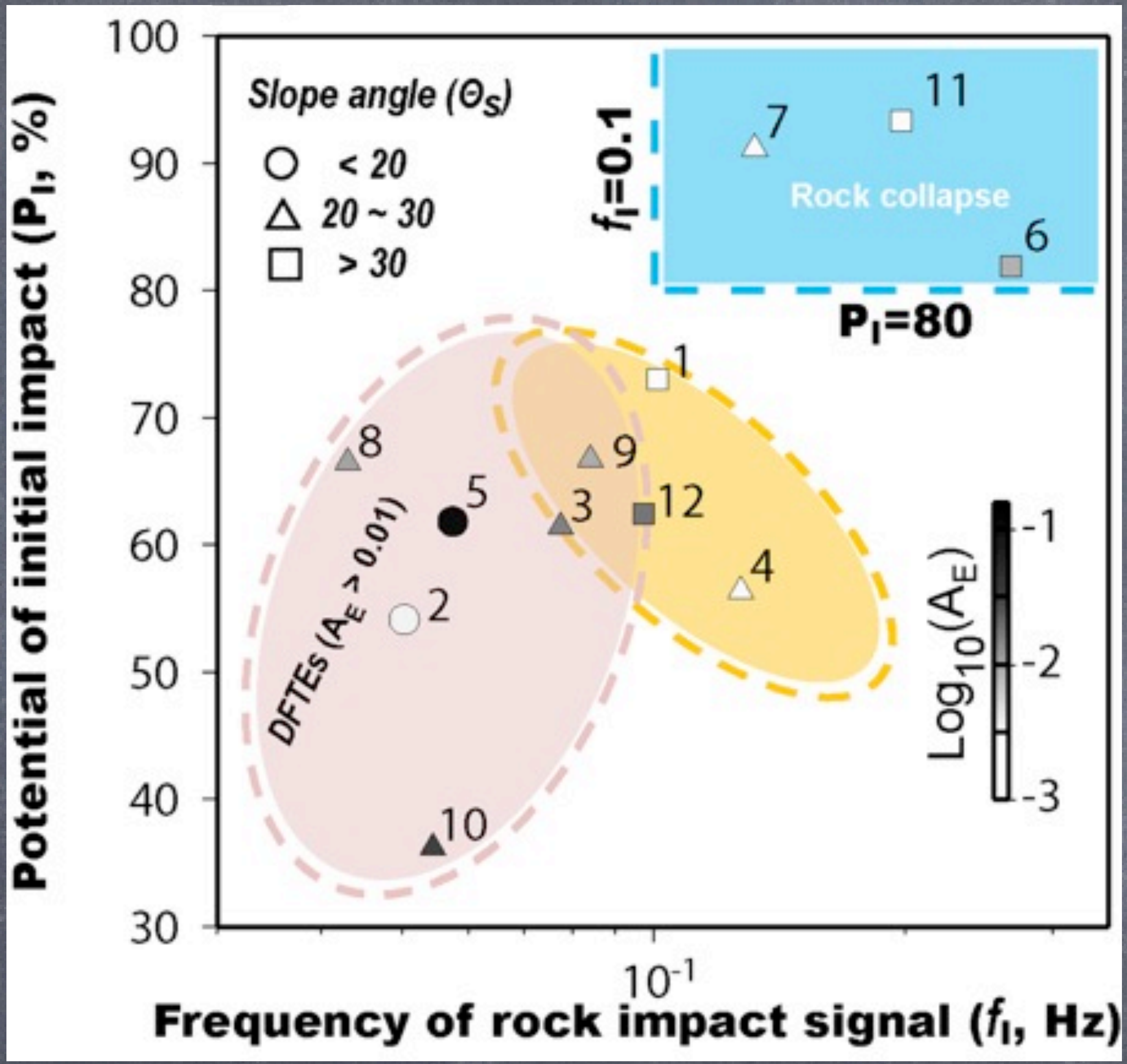

Potential of initial impact (P_I, %) = $(1-T_R/S_D) \times 100$ %

Frequency of rock impact signal (F_I, Hz) = PGV / A_E

DFTEs (Dam-formation-type events)

Summary

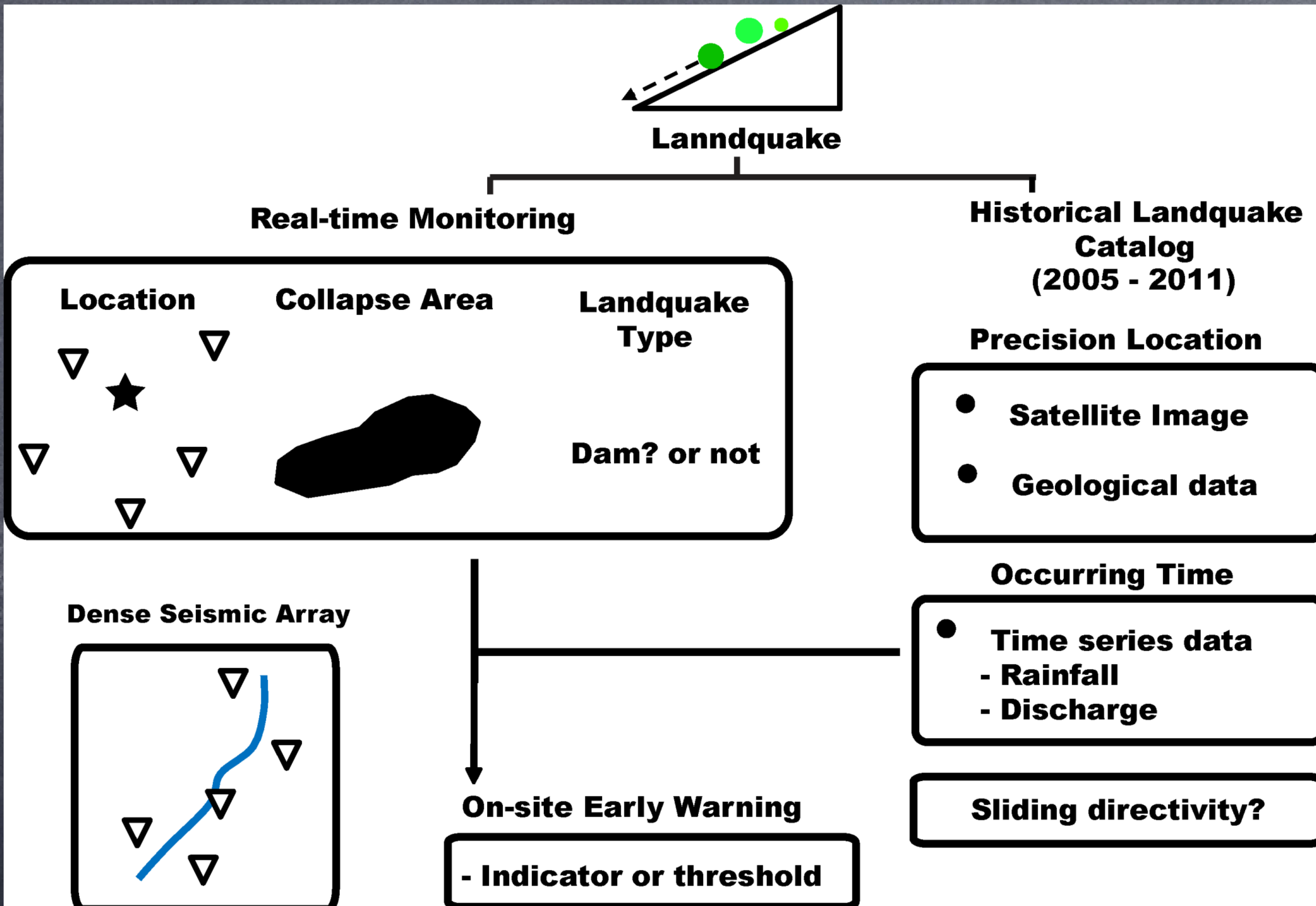

14年12月26日星期五

Dynamic processes of the landquakes from long- and short-period seismic signal analysis

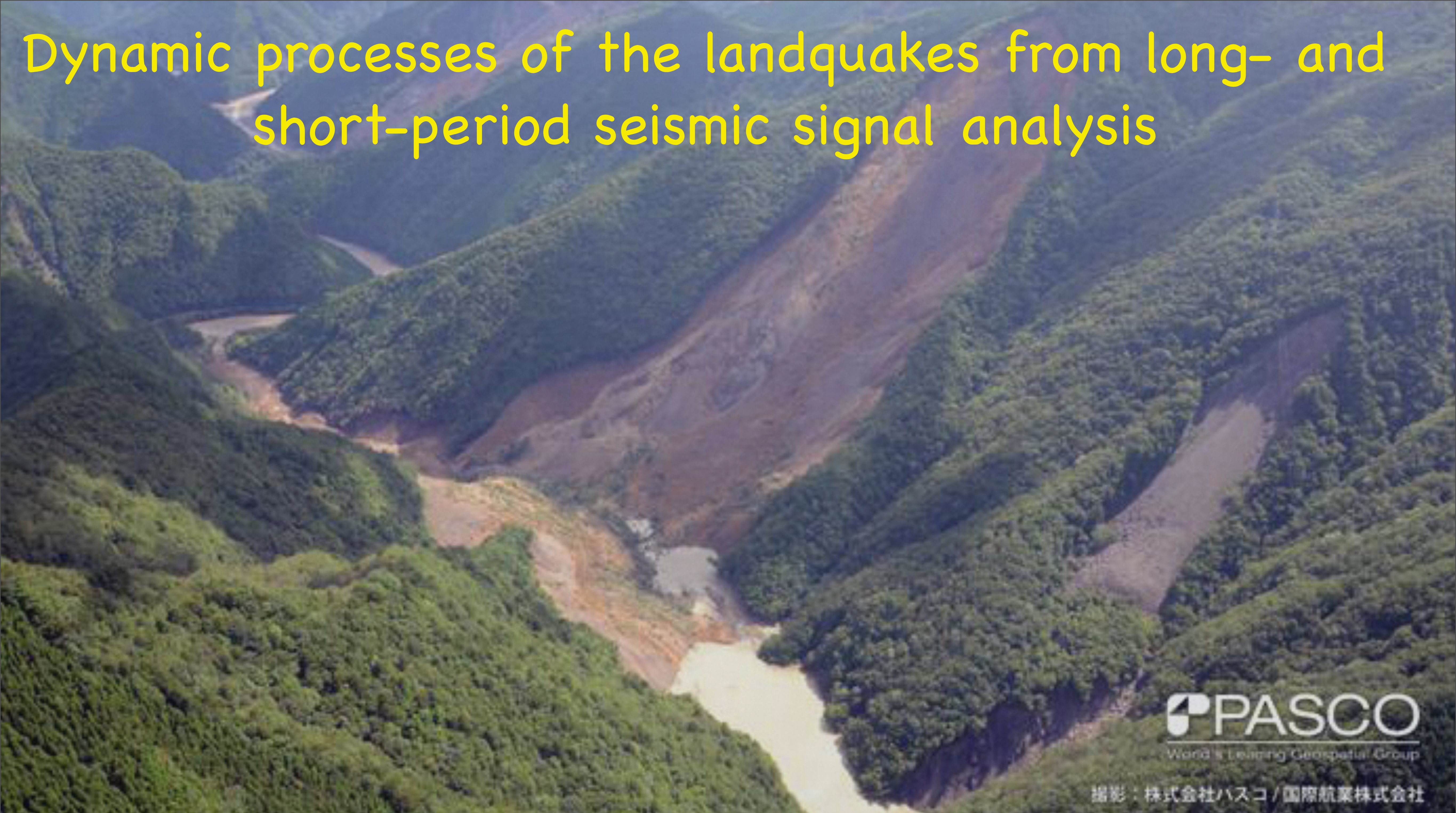

Chao et al. (2014, in preparation)

Motivations

In a past decade, seismology has provided a way to infer the dynamics of large mass movements from long-period (10-150 sec) seismic singals.

(e.g., Brodsky et al., 2003; Lin et al., 2010; Yamada et al., 2013; Ektröm & Stark, 2013; Hibert et al., 2014)

Simple Scaling of Catastrophic Landslide Dynamics
Göran Ekström and Colin P. Stark
Science **339**, 1416 (2013);
DOI: 10.1126/science.1232887

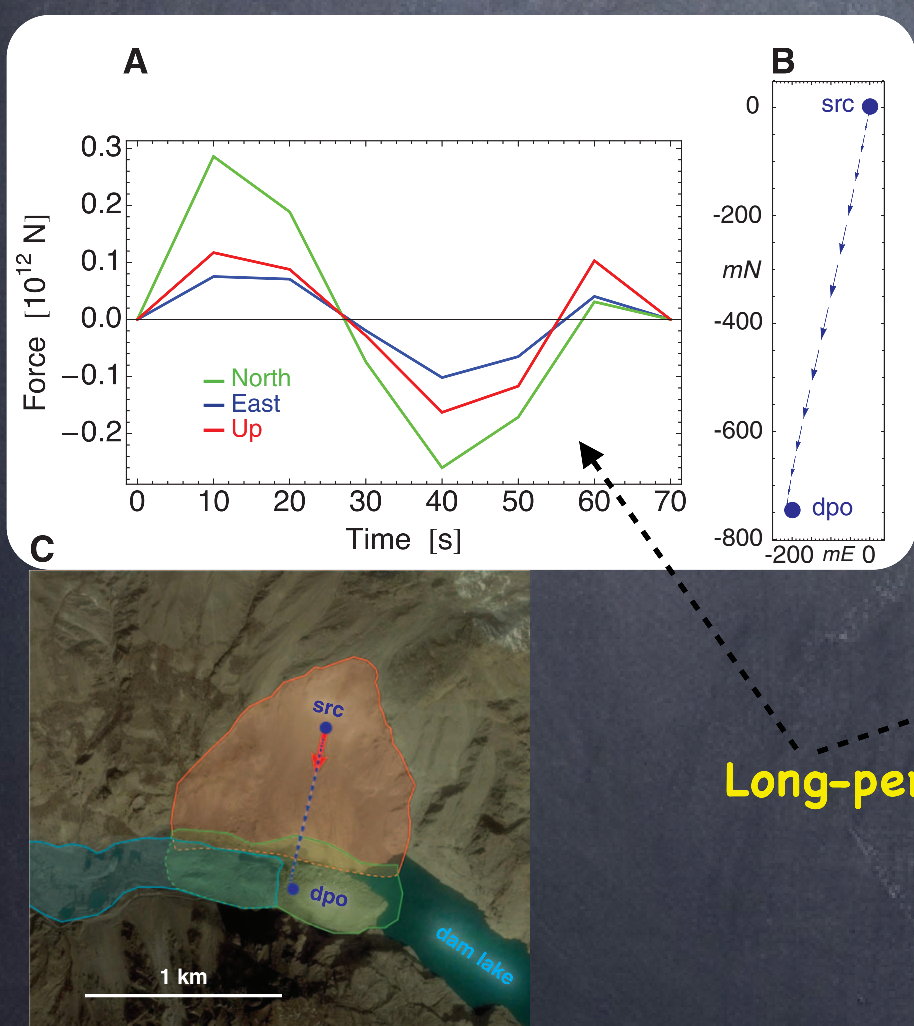

Nat. Hazards Earth Syst. Sci. Discuss., 2, 7309–7327, 2014
www.nat-hazards-earth-syst-sci-discuss.net/2/7309/2014/
doi:10.5194/nhessd-2-7309-2014
© Author(s) 2014. CC Attribution 3.0 License.

Natural Hazards and Earth System Sciences

Open Access

Seismology of the Oso-Steelhead landslide

C. Hibert, C. P. Stark, and G. Ekström

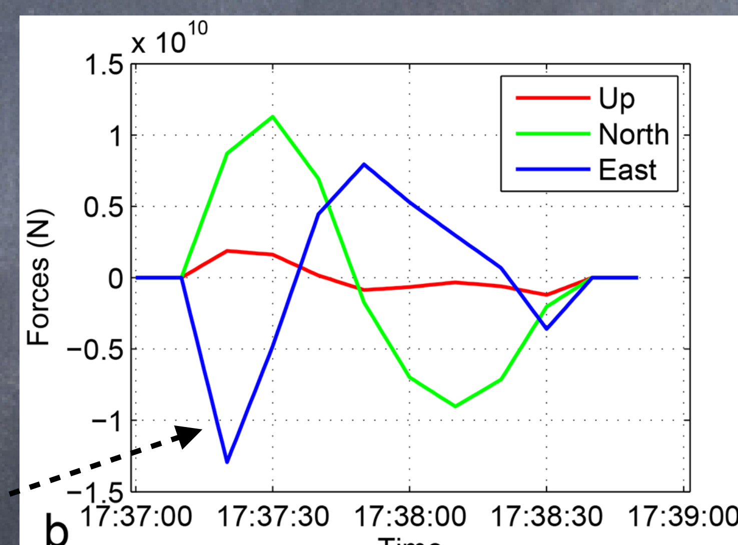

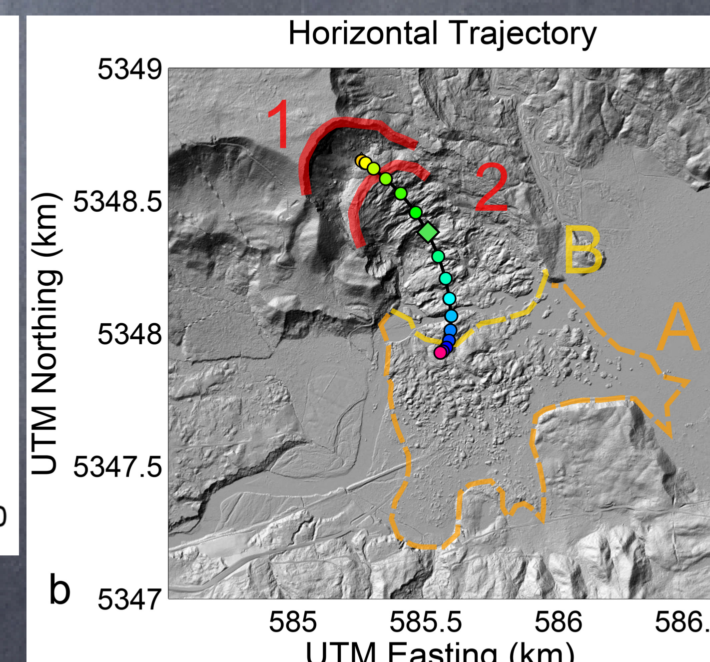

Long-period force acts on the Earth

Source mechanisms of landquake & earthquake

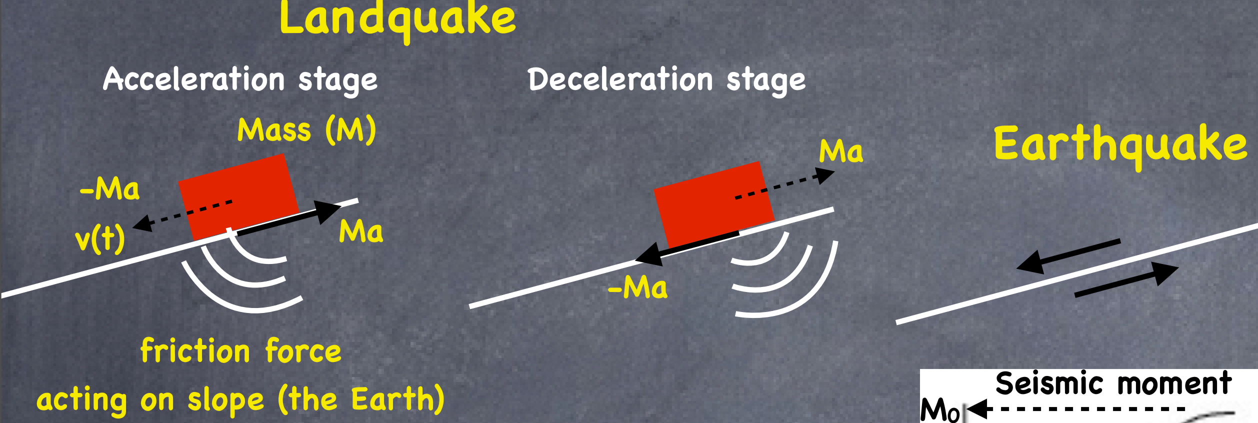

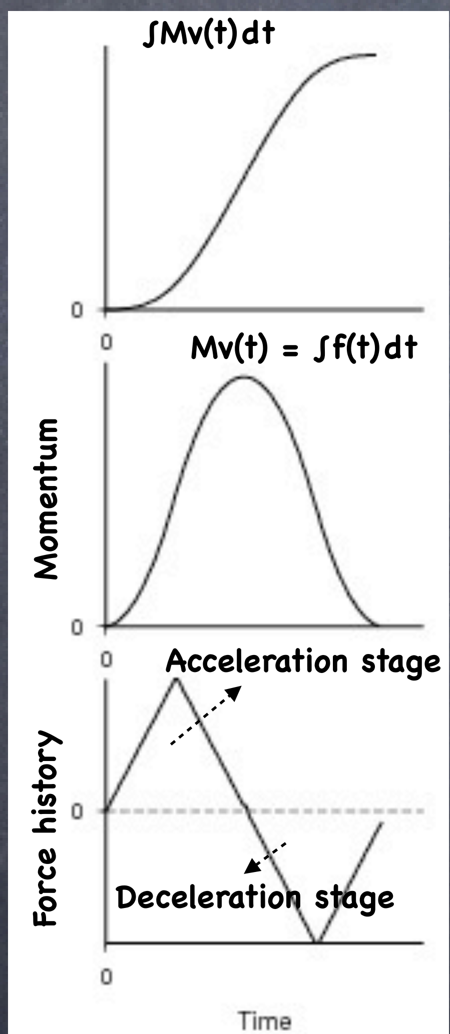

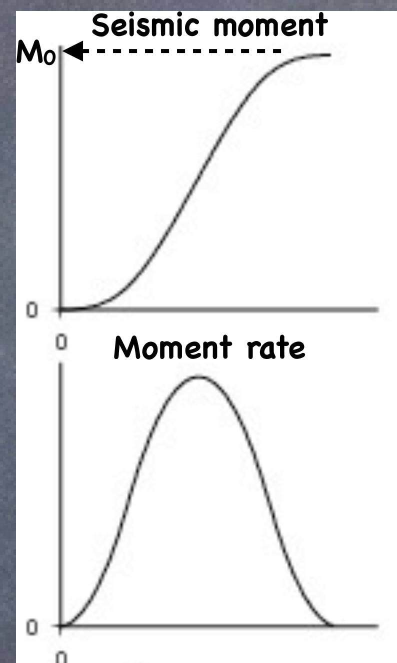

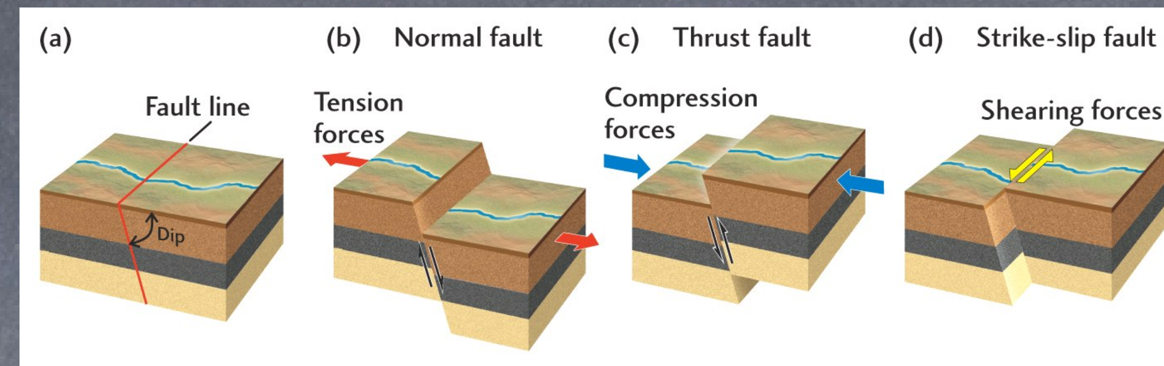

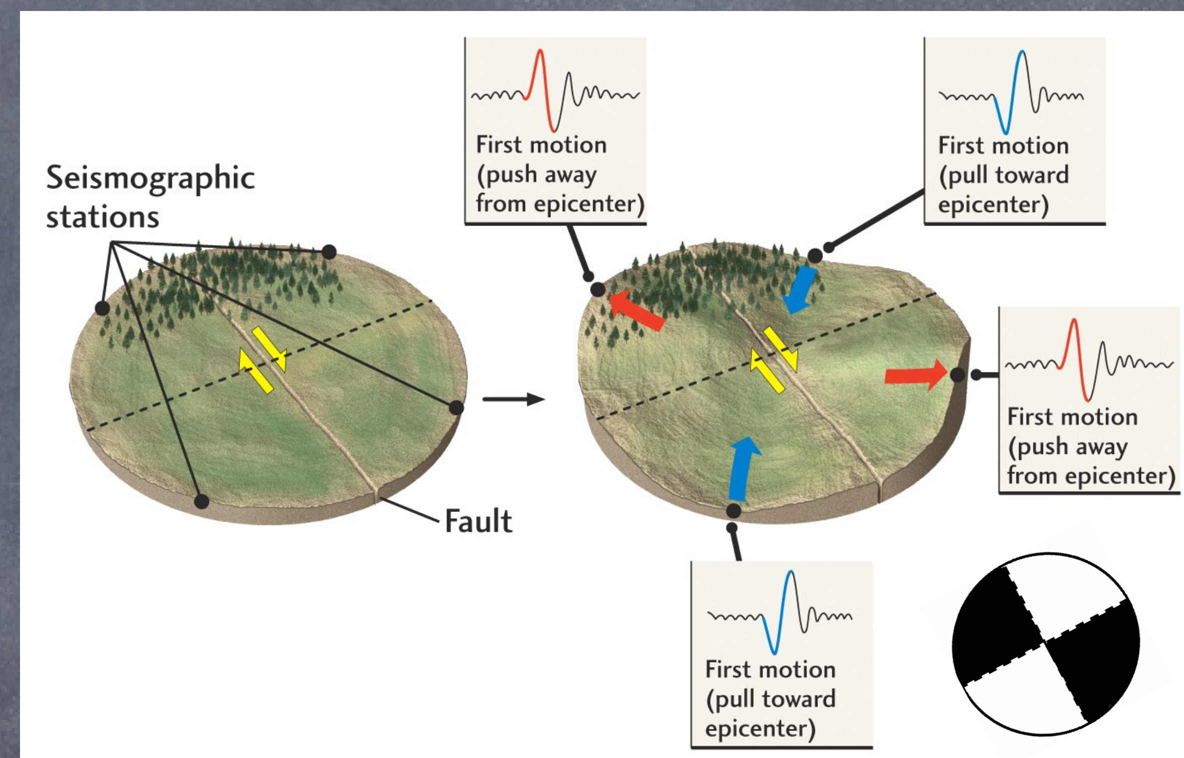

The acceleration and deceleration of the bulk mass during the landquake cause a loading and unloading of the slope that generated long-period seismic waves.

General source inversion (ASCII) algorithm

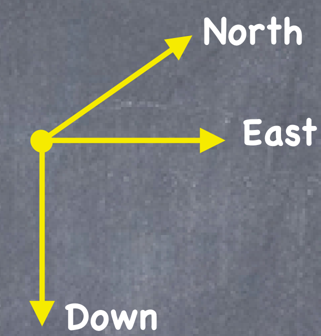

Five elementary fault-types & explosion

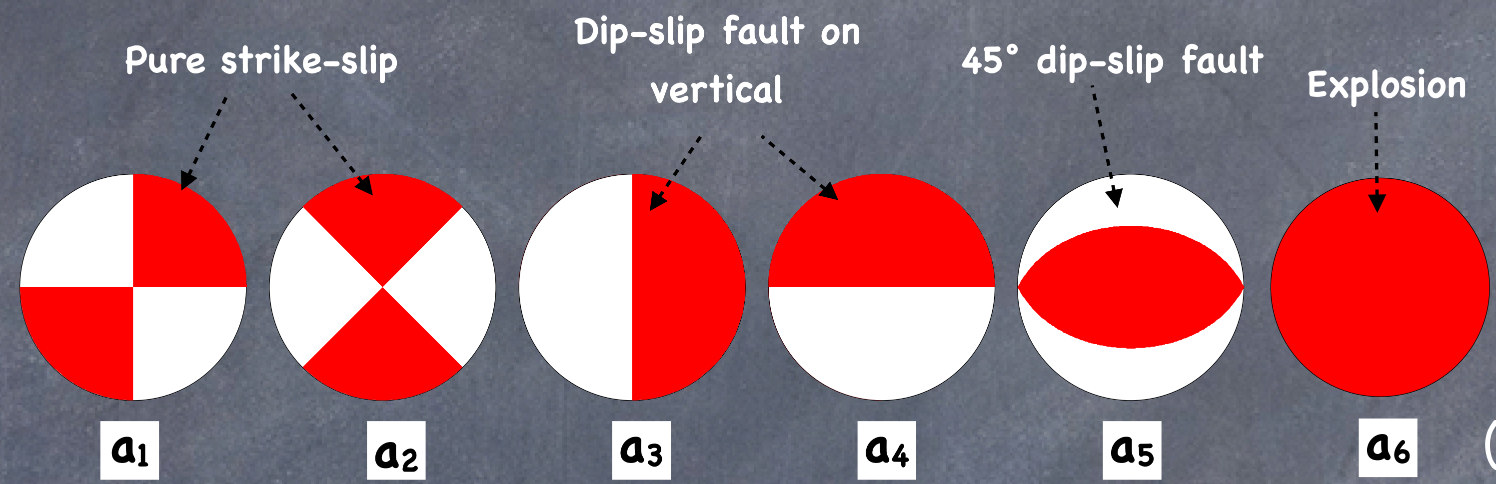

(Kikuchi & Kanamori, 1991)

$$M_1:\begin{bmatrix}0&1&0\\1&0&0\\0&0&0\end{bmatrix}\quad M_2:\begin{bmatrix}1&0&0\\0&-1&0\\0&0&0\end{bmatrix}\quad M_3:\begin{bmatrix}0&0&0\\0&0&1\\0&1&0\end{bmatrix}\quad M_4:\begin{bmatrix}0&0&1\\0&0&0\\1&0&0\end{bmatrix}\quad M_5:\begin{bmatrix}-1&0&0\\1&0&0\\0&0&1\end{bmatrix}\quad M_6:\begin{bmatrix}1&0&0\\0&1&0\\0&0&1\end{bmatrix}$$

$$M_{ij}=\sum_{n=1}^{6}A_nM_n\ ;\quad M_{ij}=\begin{bmatrix}A_2-A_5+A_6 & A_1 & A_4\\ A_1 & -A_2+A_6 & A_3\\ A_4 & A_3 & A_5+A_6\end{bmatrix}$$

Three orthogonal forces (two horizontal forces & one vertical force)

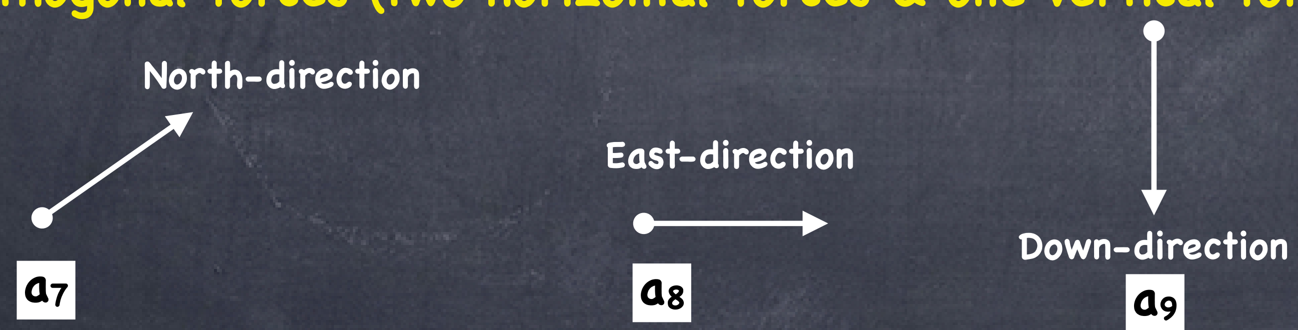

Synthetic seismograms

The Green's Functions (G) are calculated using a numerical implementation of the propagator-matrix approach (e.g. fk3.0 software package; Zhu and Rivera, 2002).

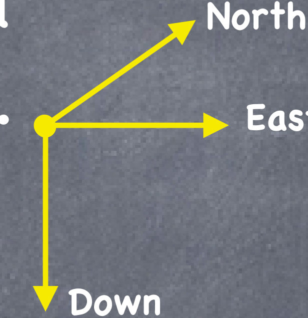

$$g^n(t,\vec{x}) = M_{ij} \cdot G_{ni,j}(t,\vec{x})$$

$$U^z(x,t) = \sum_{m=1}^{9} a_m g_m^z(x,t)$$

$$U^r(x,t) = \sum_{m=1}^{9} a_m g_m^r(x,t)$$

$$U^t(x,t) = \sum_{m=1}^{9} a_m g_m^t(x,t)$$

Five elementary fault-types & explosion

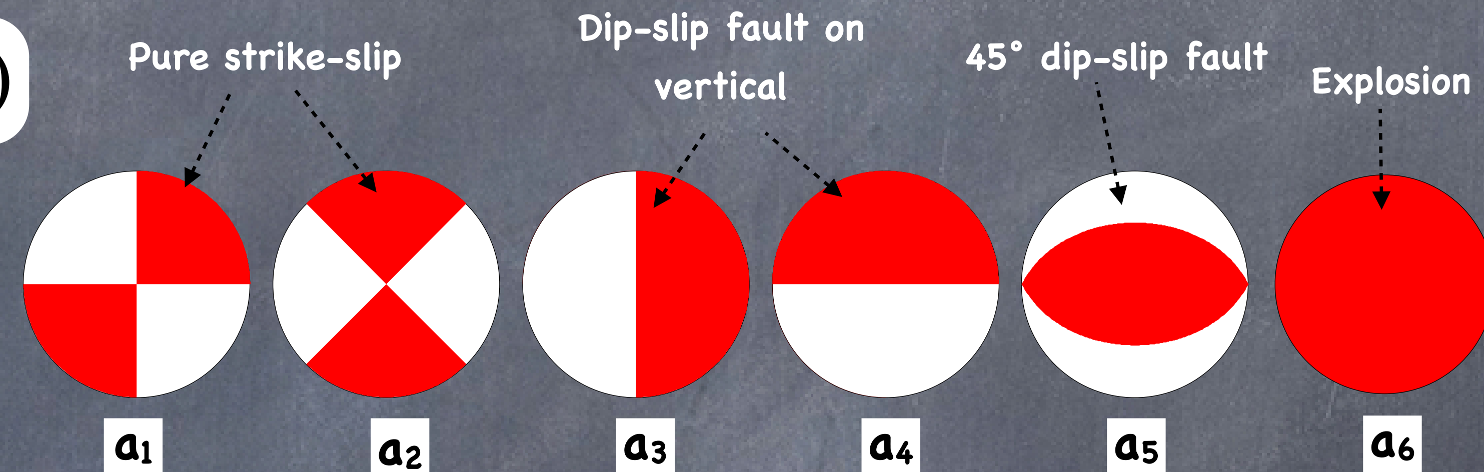

$$M_1 : \begin{bmatrix} 0 & 1 & 0 \\ 1 & 0 & 0 \\ 0 & 0 & 0 \end{bmatrix} \quad M_2 : \begin{bmatrix} 1 & 0 & 0 \\ 0 & -1 & 0 \\ 0 & 0 & 0 \end{bmatrix} \quad M_3 : \begin{bmatrix} 0 & 0 & 0 \\ 0 & 0 & 1 \\ 0 & 1 & 0 \end{bmatrix} \quad M_4 : \begin{bmatrix} 0 & 0 & 1 \\ 0 & 0 & 0 \\ 1 & 0 & 0 \end{bmatrix} \quad M_5 : \begin{bmatrix} -1 & 0 & 0 \\ 1 & 0 & 0 \\ 0 & 0 & 1 \end{bmatrix} \quad M_6 : \begin{bmatrix} 1 & 0 & 0 \\ 0 & 1 & 0 \\ 0 & 0 & 1 \end{bmatrix}$$

$$M_{ij} = \sum_{n=1}^{6} A_n M_n \quad ; \quad M_{ij} = \begin{bmatrix} A_2 - A_5 + A_6 & A_1 & A_4 \\ A_1 & -A_2 + A_6 & A_3 \\ A_4 & A_3 & A_5 + A_6 \end{bmatrix}$$

Three orthogonal forces (two horizontal forces & one vertical force)

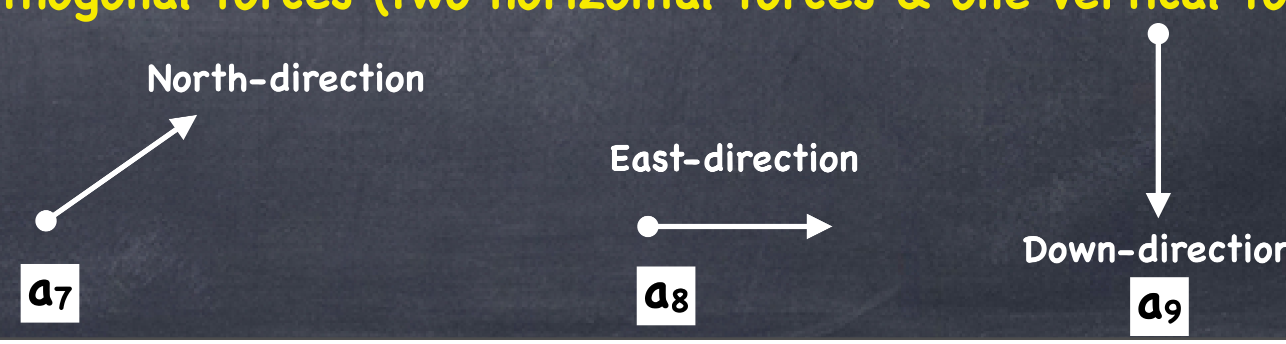

Variance reduction (VR) & Fitness

Normalized cross-correlation coefficient

$$NCC = \frac{C_{os}}{\sqrt{C_{oo}C_{ss}}}$$

C_{os}: the maximum observed-synthetic cross-correlation coefficient

C_{oo}, C_{ss}: the maximum autocorrelation coefficient

Variance reduction (VR)

$$VR = 1 - \frac{\sum_{i=1}^{np}(obs_i - syn_i)^2}{\sum_{i=1}^{np} obs_i^2}$$

so if observed = synthetic, VR = 1

synthetic = 0, VR = 0

observed = -synthetic, VR = -3

Fitness= Avg. NCC + Avg. VR

Earthquake? or Explosion?

earthquake-type Fitness: 0.7884 Mw=3.70

CLVD: 55.33% DC: 44.67%

isotropic-type Fitness: 0.6619 Mw=3.81

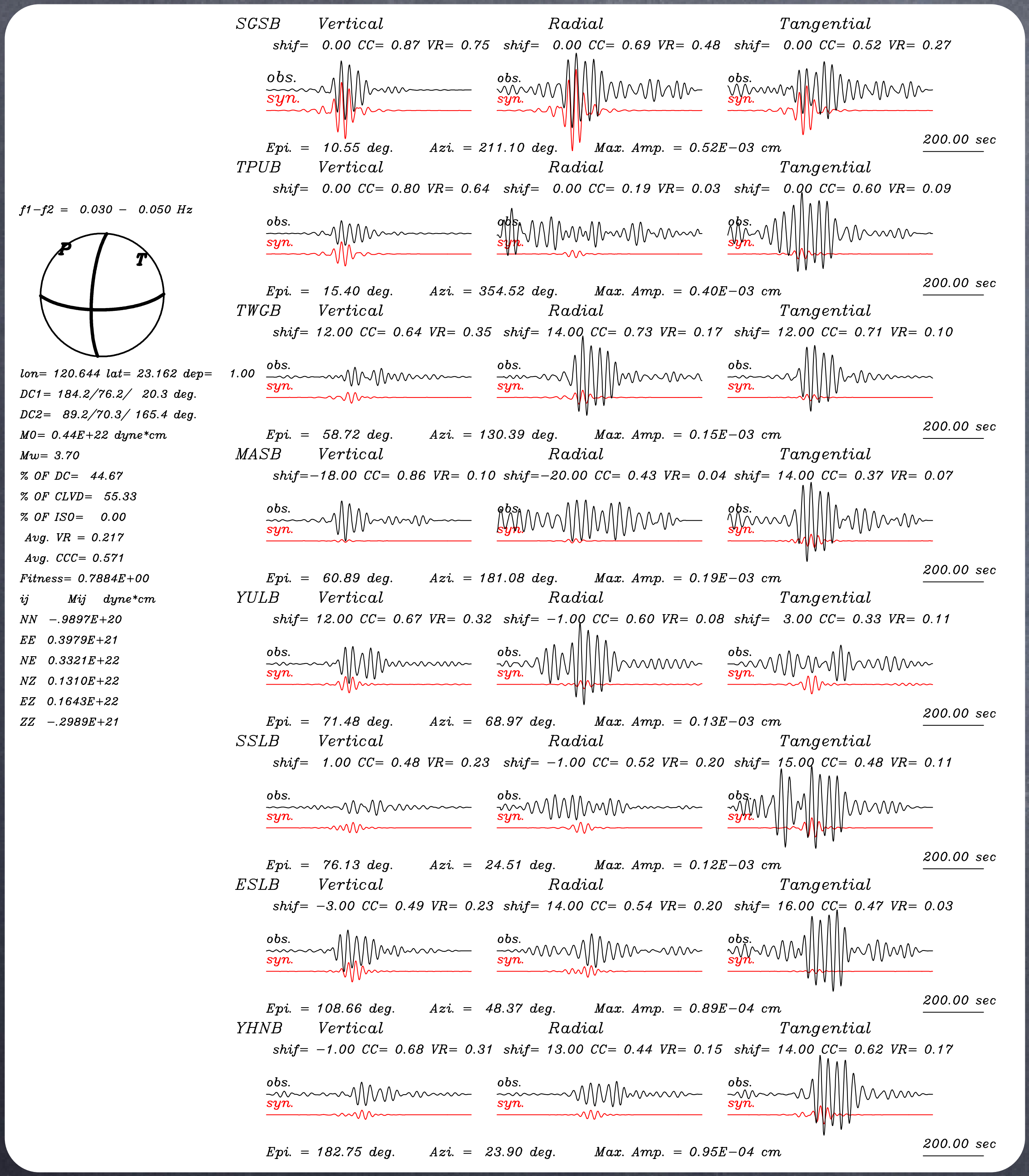

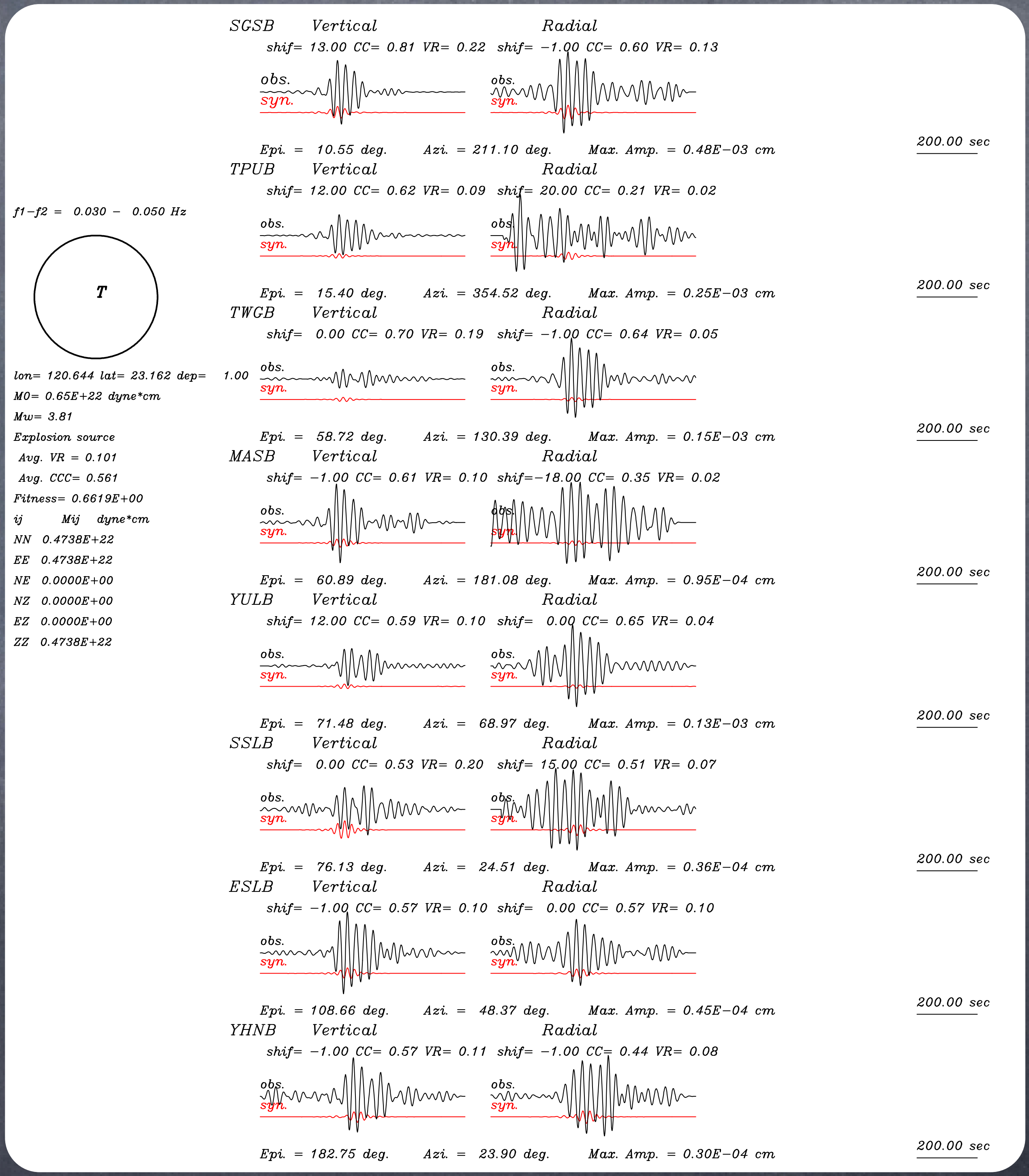

What waveforms tell you?

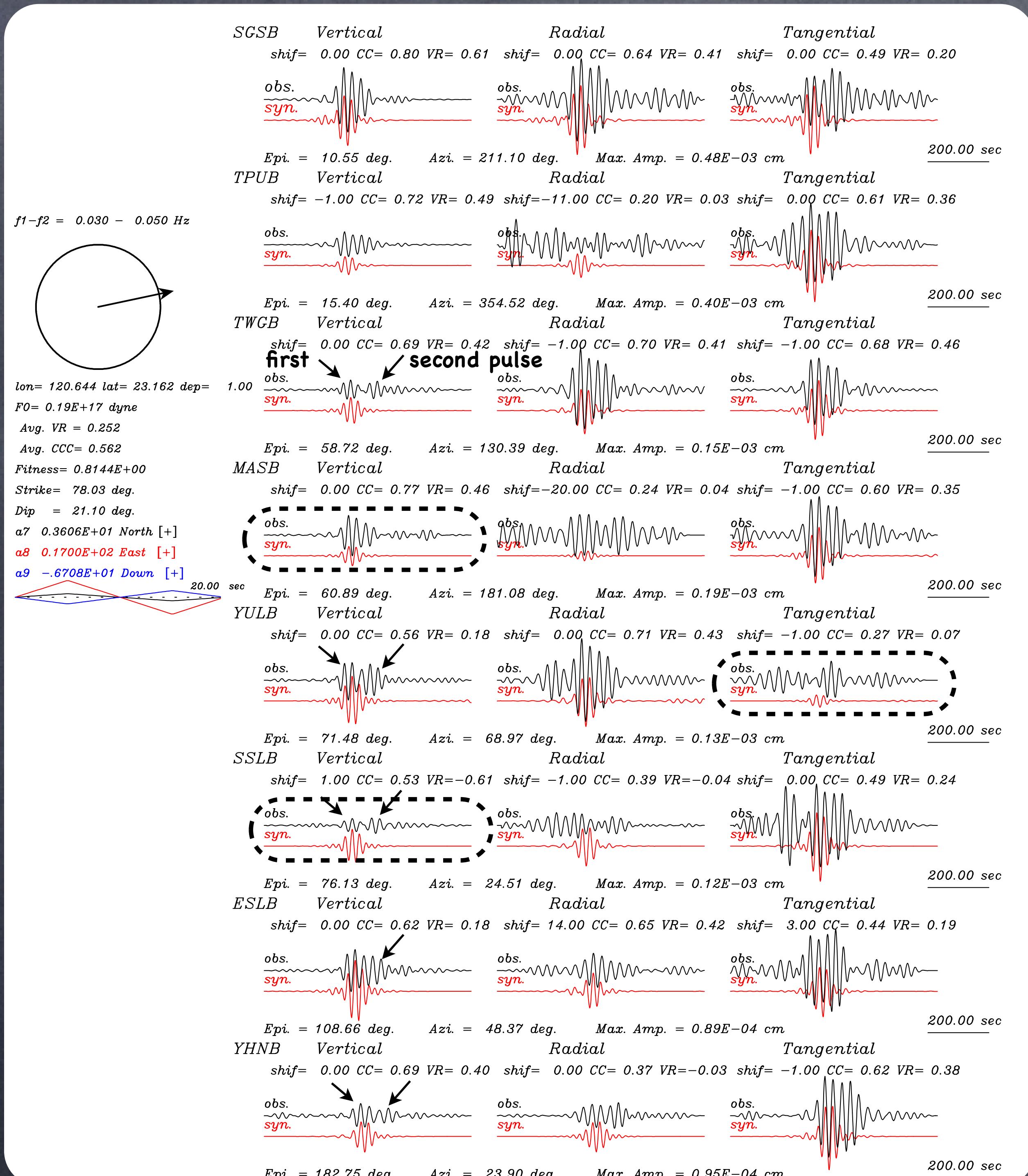

Multiple force vector from long-period signals

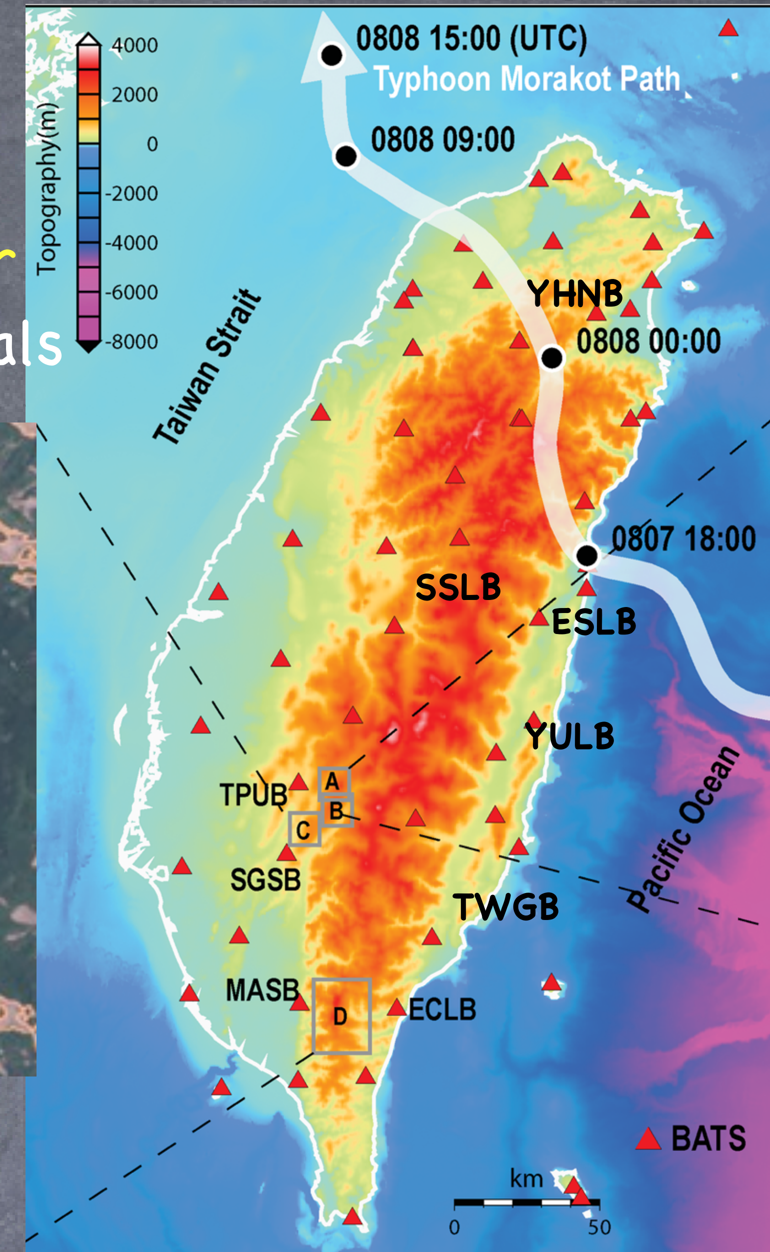

Topography changes (Kuo et al. 2011)

Collapse area = 2.48 km²

Estimated volume = 25 x 10⁶ m³

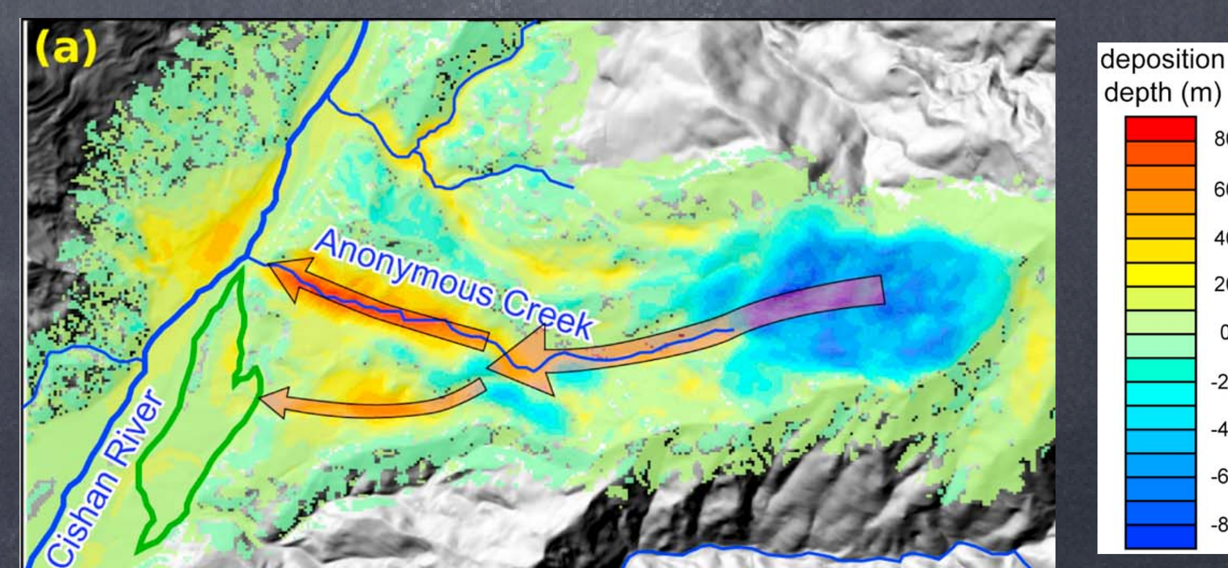

Force strike: 78°

Single force-type Fitness: 0.8144

Force angle: 21° (field measurement: avg. 18°)

Force magnitude: 1.86×10^{11} N

1.10×10^{11} N (Ekström & Stark, 2013) 35-150 sec filtered

0.50×10^{11} N (Lin et al., 2010) 50-100 sec filtered

What waveforms tell you?

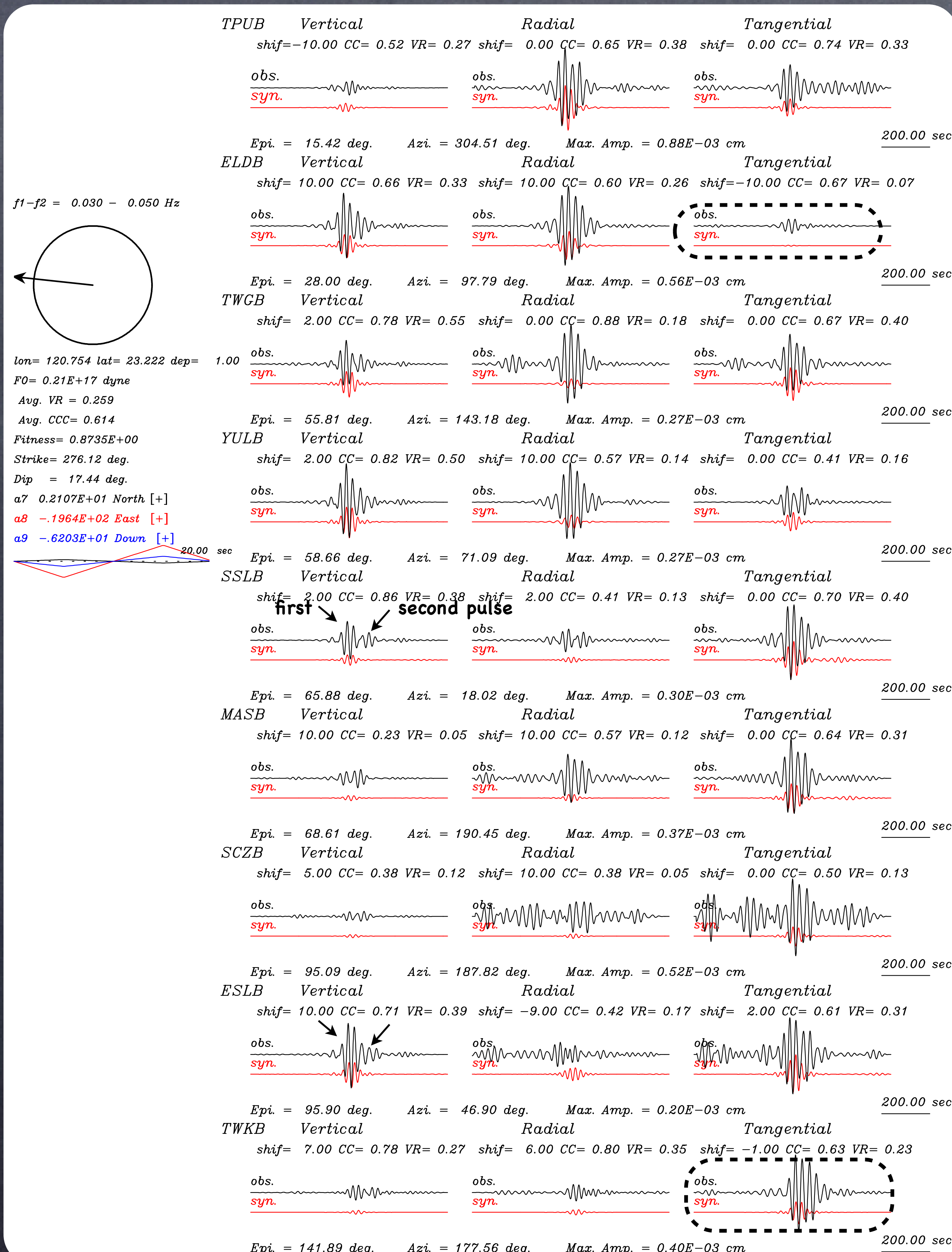

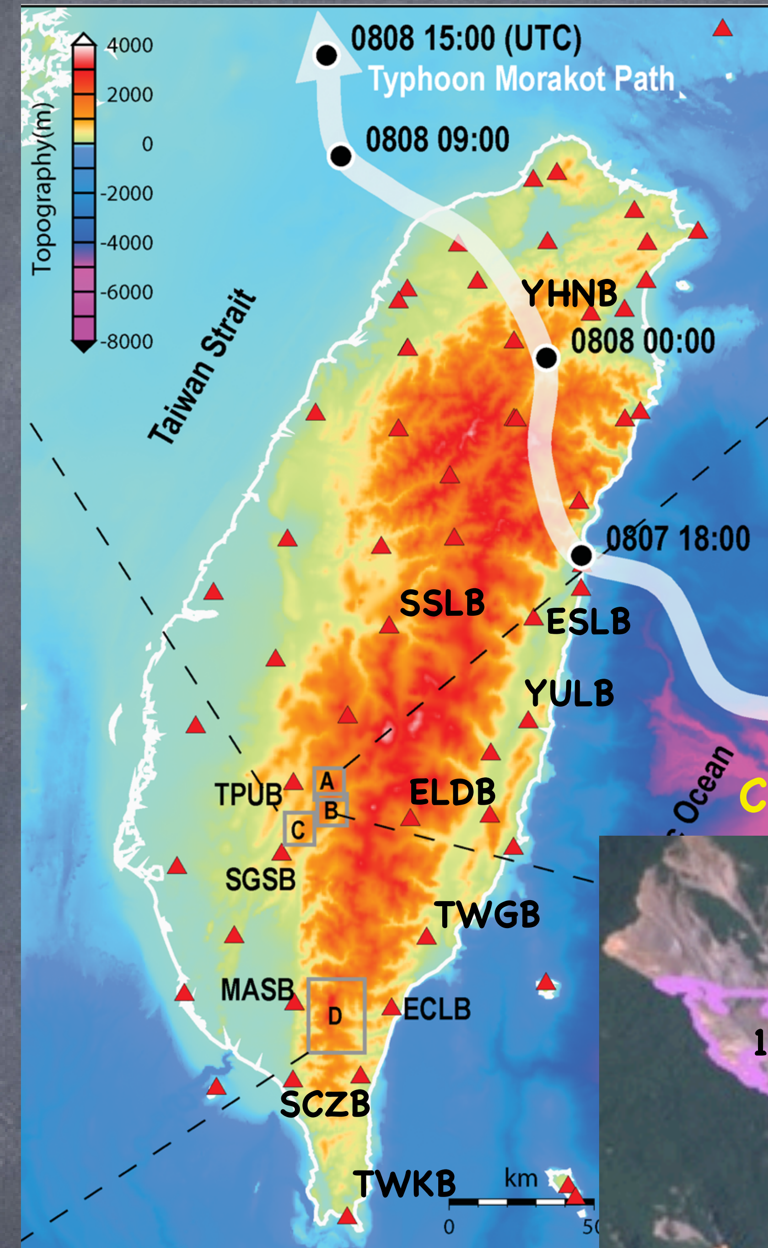

Laonong event

Collapse area = 2.02 km^2

Force strike: 276°

Force angle: 17.4° (field measurement: avg. 26°)

Force magnitude: 2.1 x 10^{11} N

Fitness: 0.8735

What waveforms tell you?

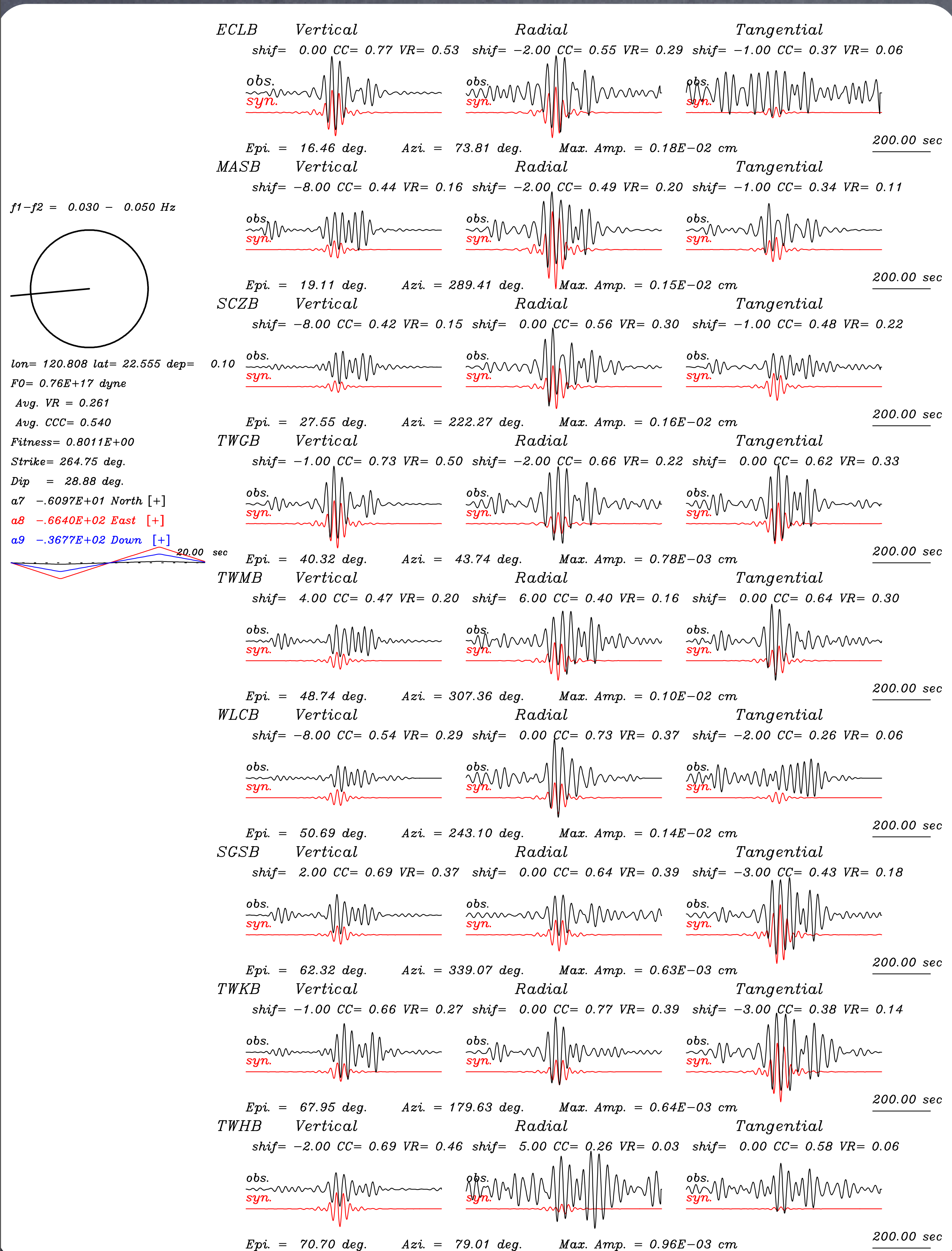

Taimali event

Collapse area = 2.27 km²

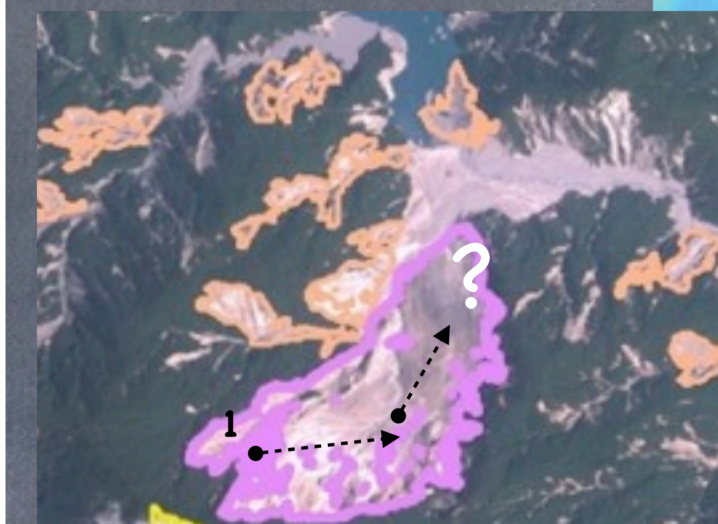

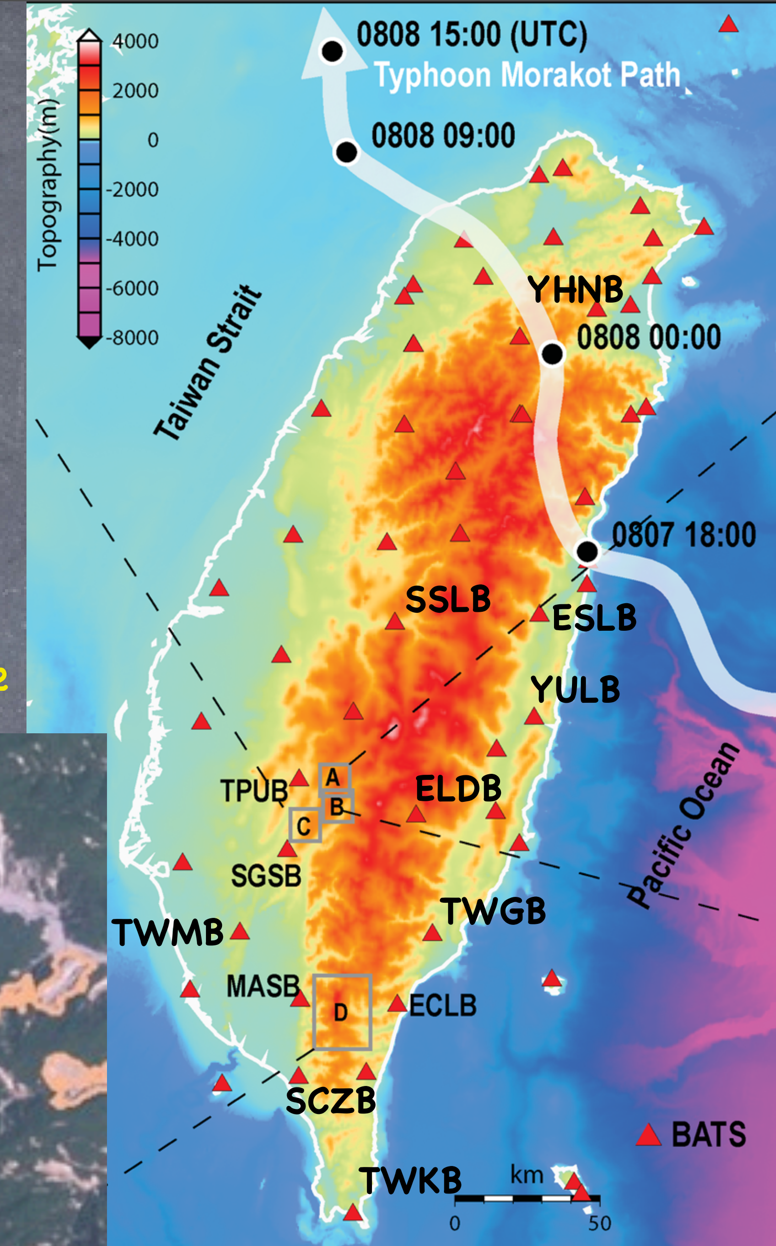

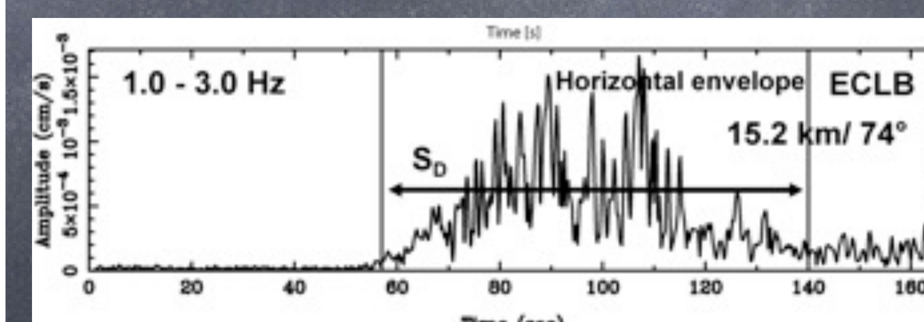

Force strike: 264°

Force angle: 28.9° (field measurement: avg. 25°)

Force magnitude: 7.6 x 10^{11} N

Fitness: 0.8011

Seismologically determined bedload flux during the typhoon season

Chao et al. (Scientific Reports; revised)

Motivations

Sediment transport and bedrock incision are critical parameters in studies of the landscape evolution and are needed for flood hazard mitigation.

However, most of conventional geomorphic methods are in situ and can not be used during an extreme flowing water environment. Thus, no information is available during typhoon events.

A potential solution to this data gap is to use remote monitoring that is possible because geophones or seismometers capture ground vibration caused by the surface process.

(Kanamori & Given, 1982; Brodsky et al., 2003; Deparis et al., 2008; Lin et al., 2010; Yamada et al., 2013; Chen et al., 2013)

Seismic, hydrological, and meteorological data

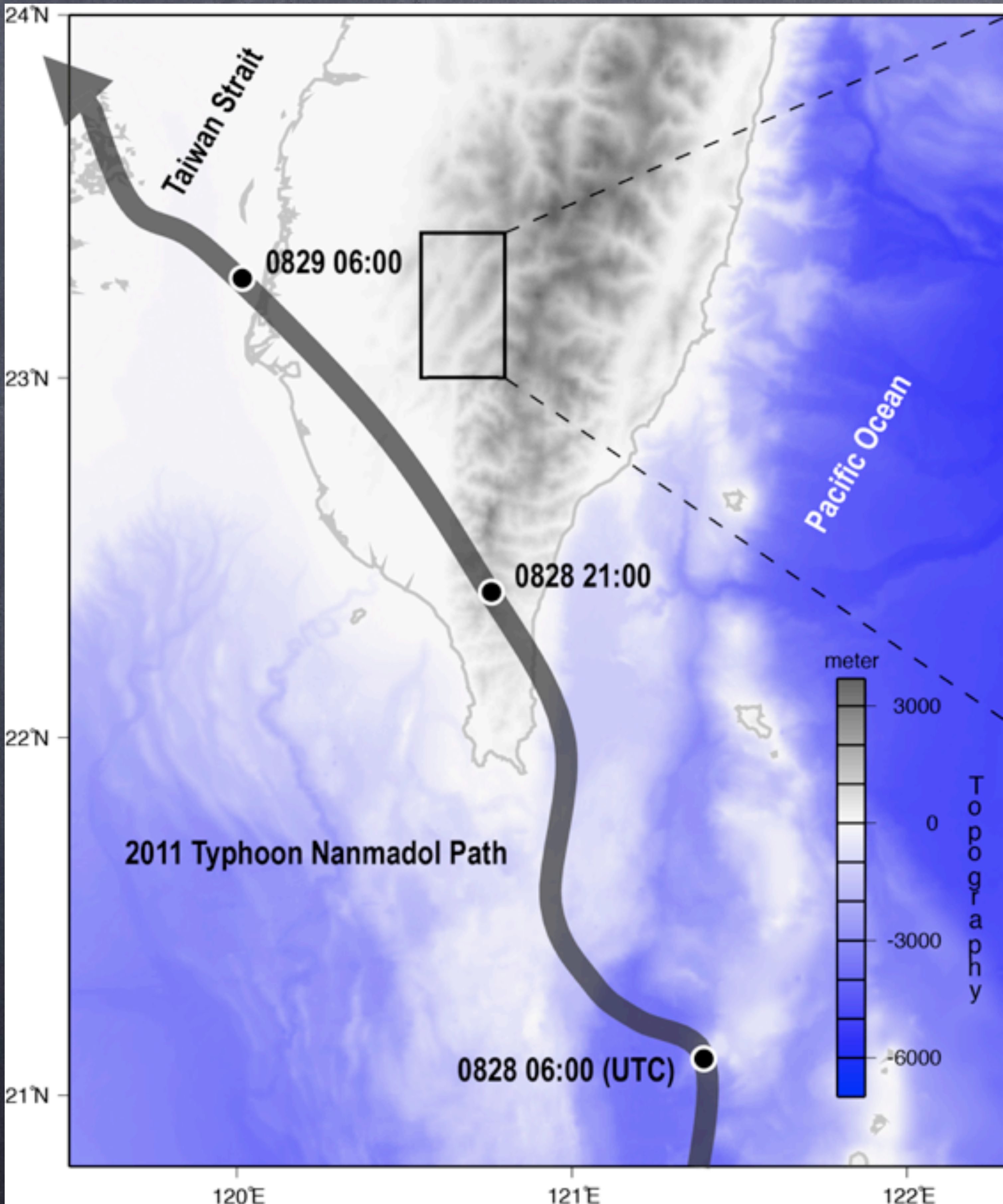

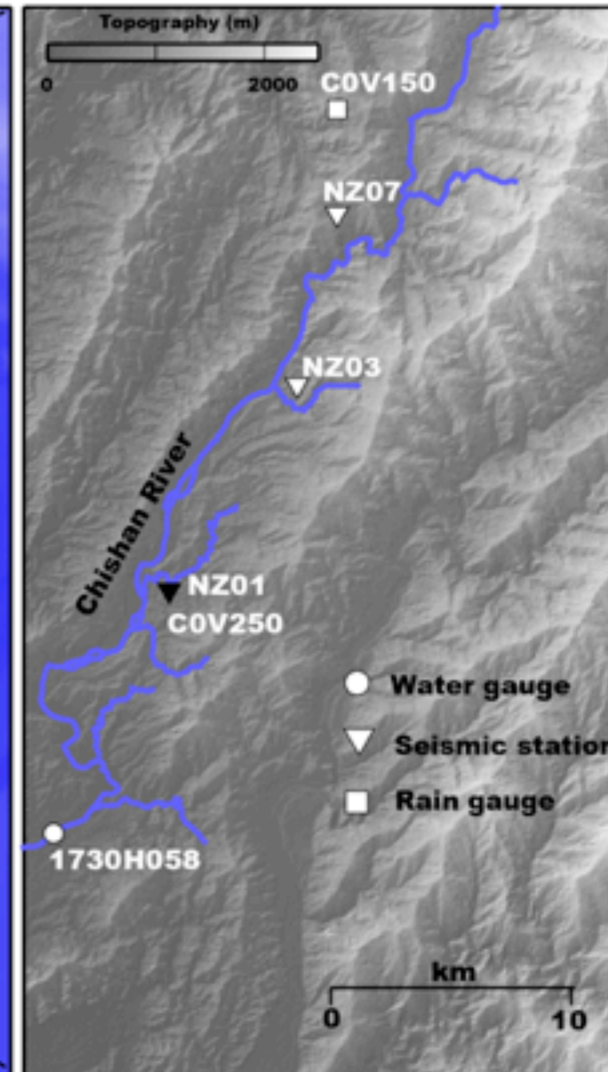

At a distance of less than 2 km from the river.

Small Typhoon event: Cumulative precipitation < 350 mm in Jiasian area.

Drains area: 842 km^2

River length: 117 km

Characteristics of river seismic noise

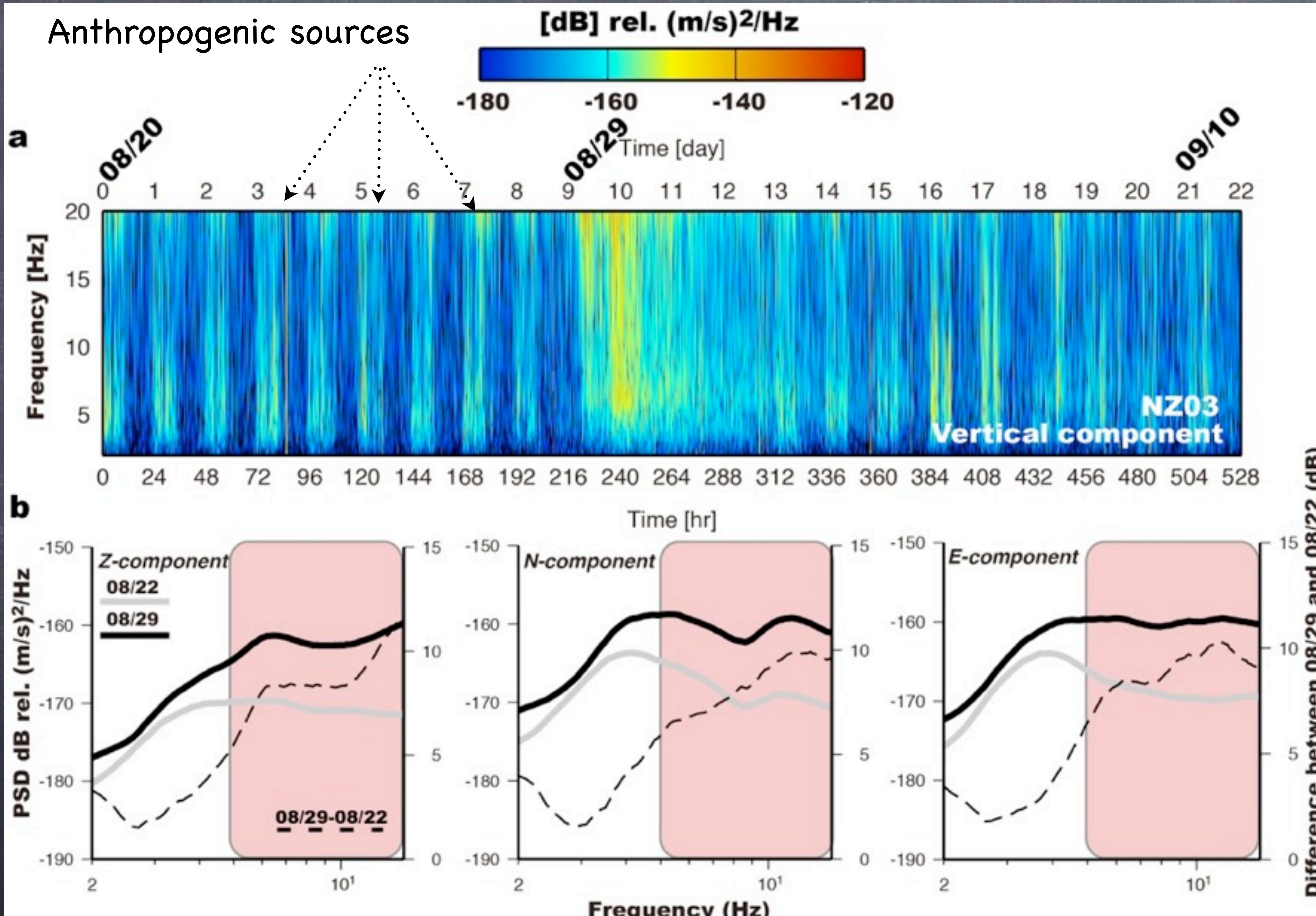

Spatial variation of the observed PSD

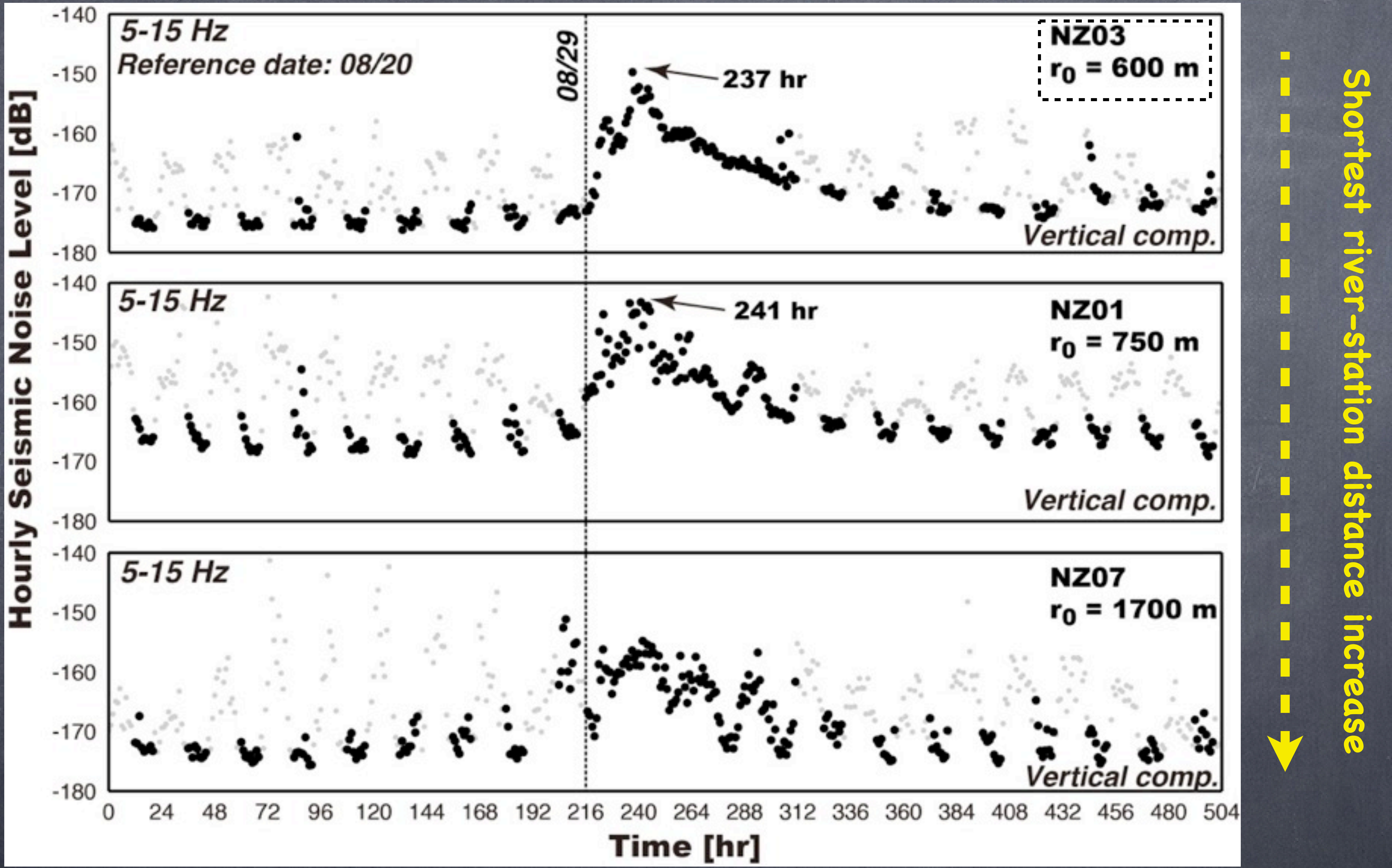

As expected, the hourly PSD during typhoon passage at NZ03 (closest to river) reveal a strong increase in the PSD amplitude.

Noise phase cross-correlation function

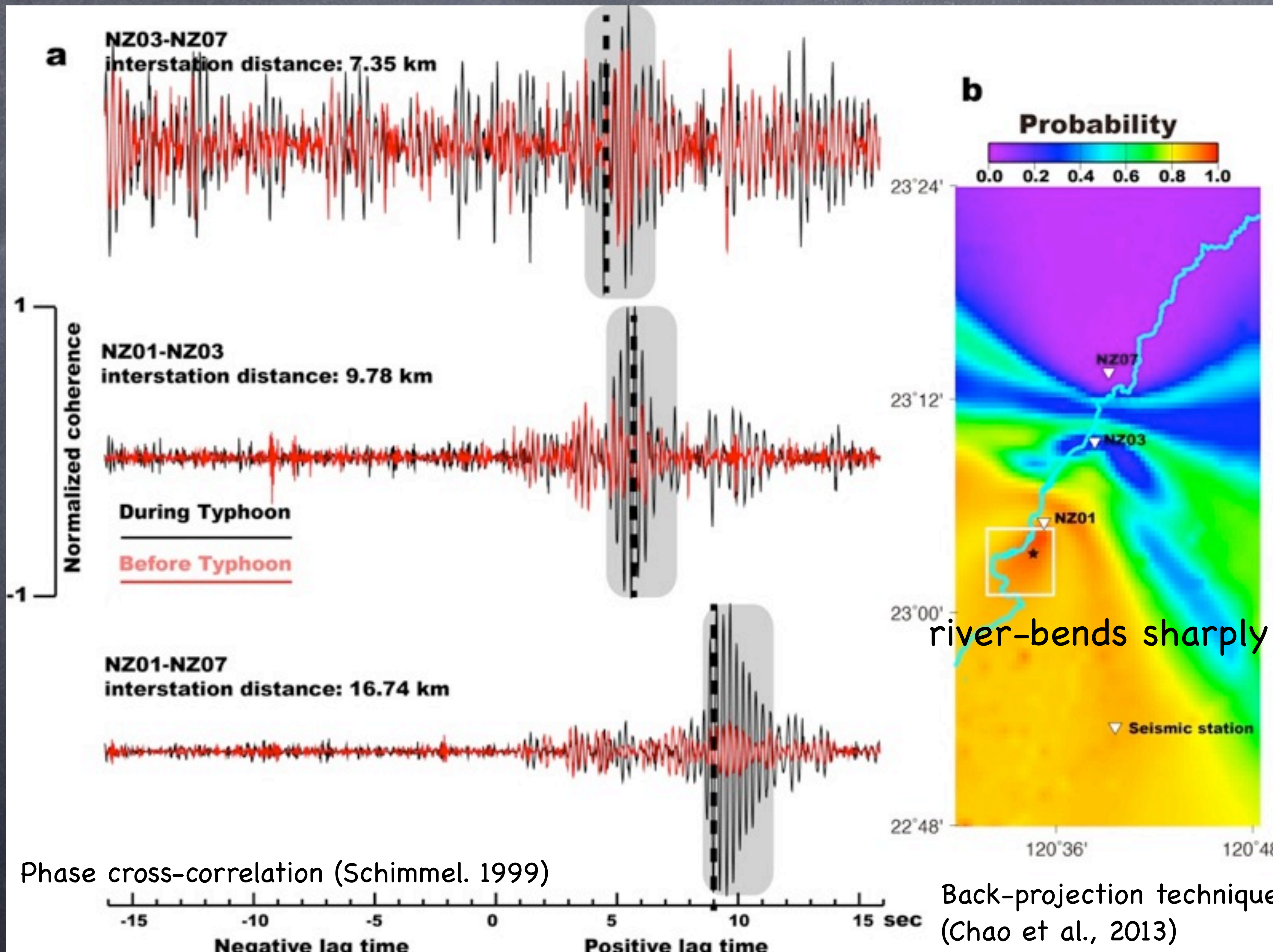

Phase cross-correlation (Schimmel. 1999)

Back-projection technique (Chao et al., 2013)

Observed hysteresis

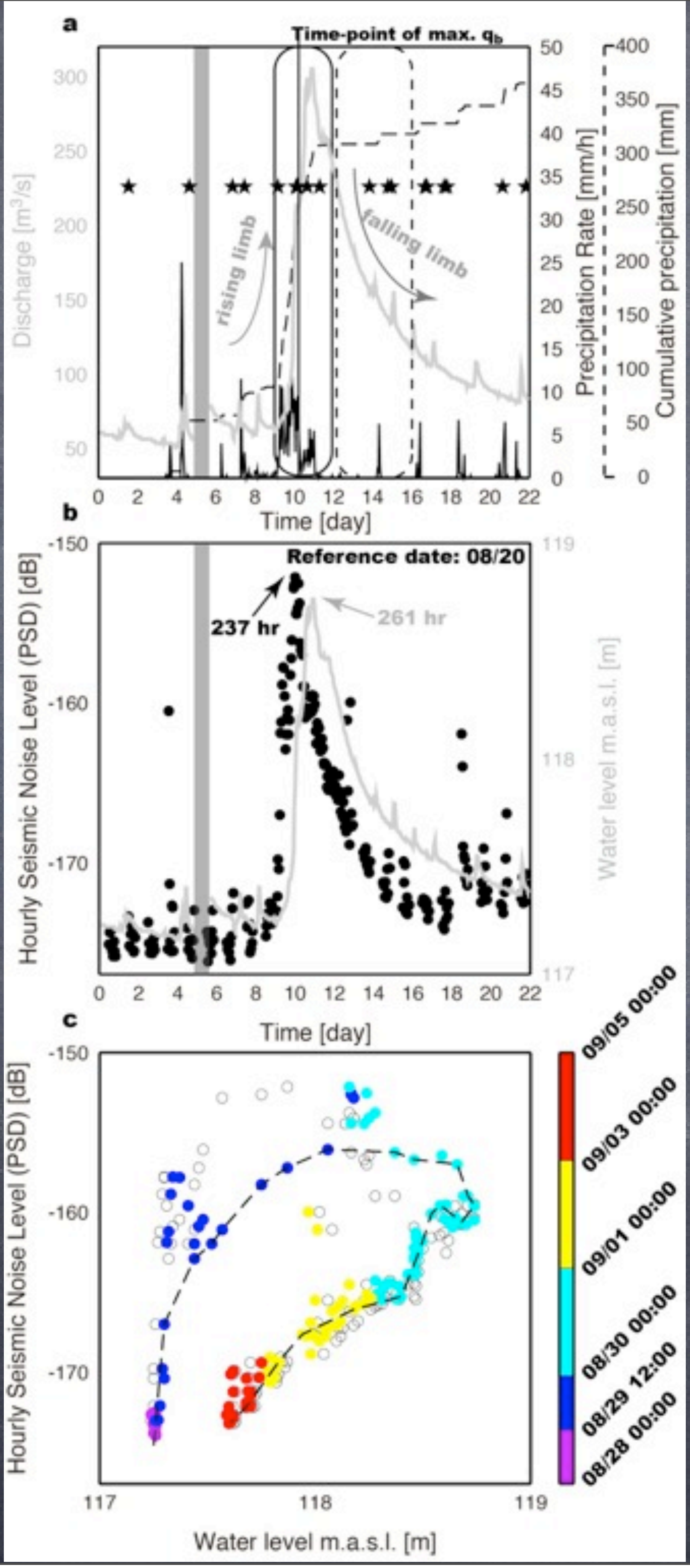

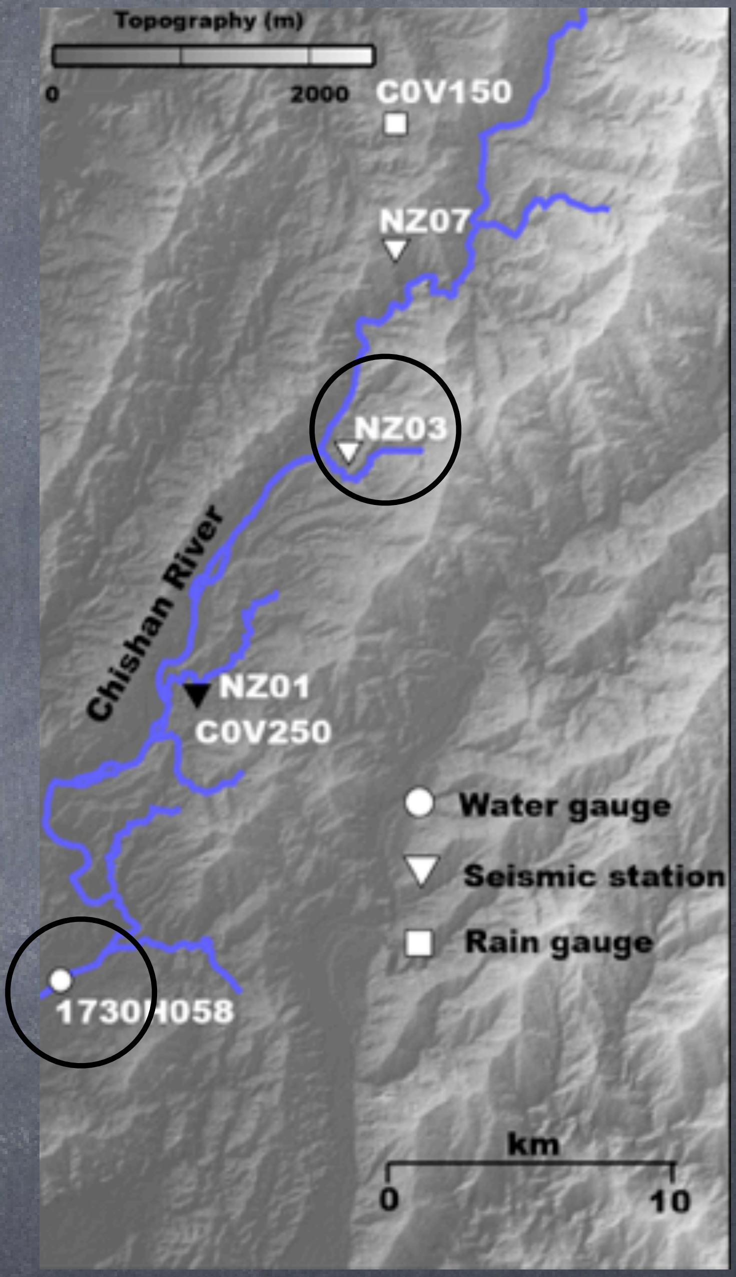

Seismologically-determined bedload flux

Results of inversion

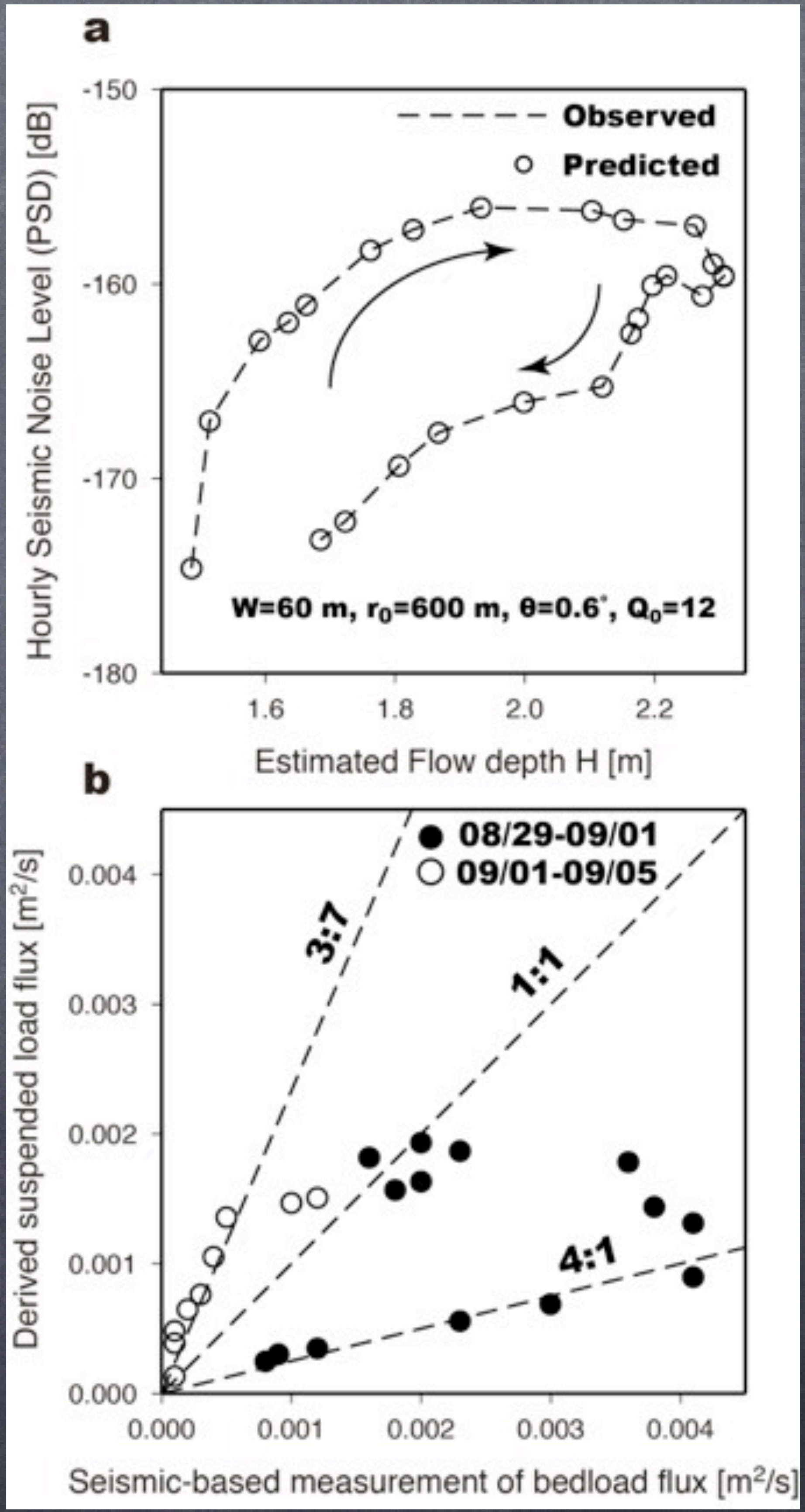

Summary of input parameters for **inversion**

Seismological compoenets (frequency-dependent):

1. Rayleigh-wave group and phase velocity (v_u, v_c) (Boore & Joyner, 1997; Ma et al., 2013)
2. Quality factor (Q_0) (Ma et al., 2013)
3. Observed *PSD* amplitude

Fluvial compoenets:

1. Flow depth of water (*H*) (WRA, 2011)
2. Geometry of channel-bed:

Width (*W*): 60 m (WRA, 2011)

Slope (θ): 0.6 degree (CGS, 2013)

3. **Grain size distribution** (CGS, 2013)

Discussion & conclusions

Temporal changes of sediment flux ratio (suspended load flux, q_s v.s. bedload flux, q_b)

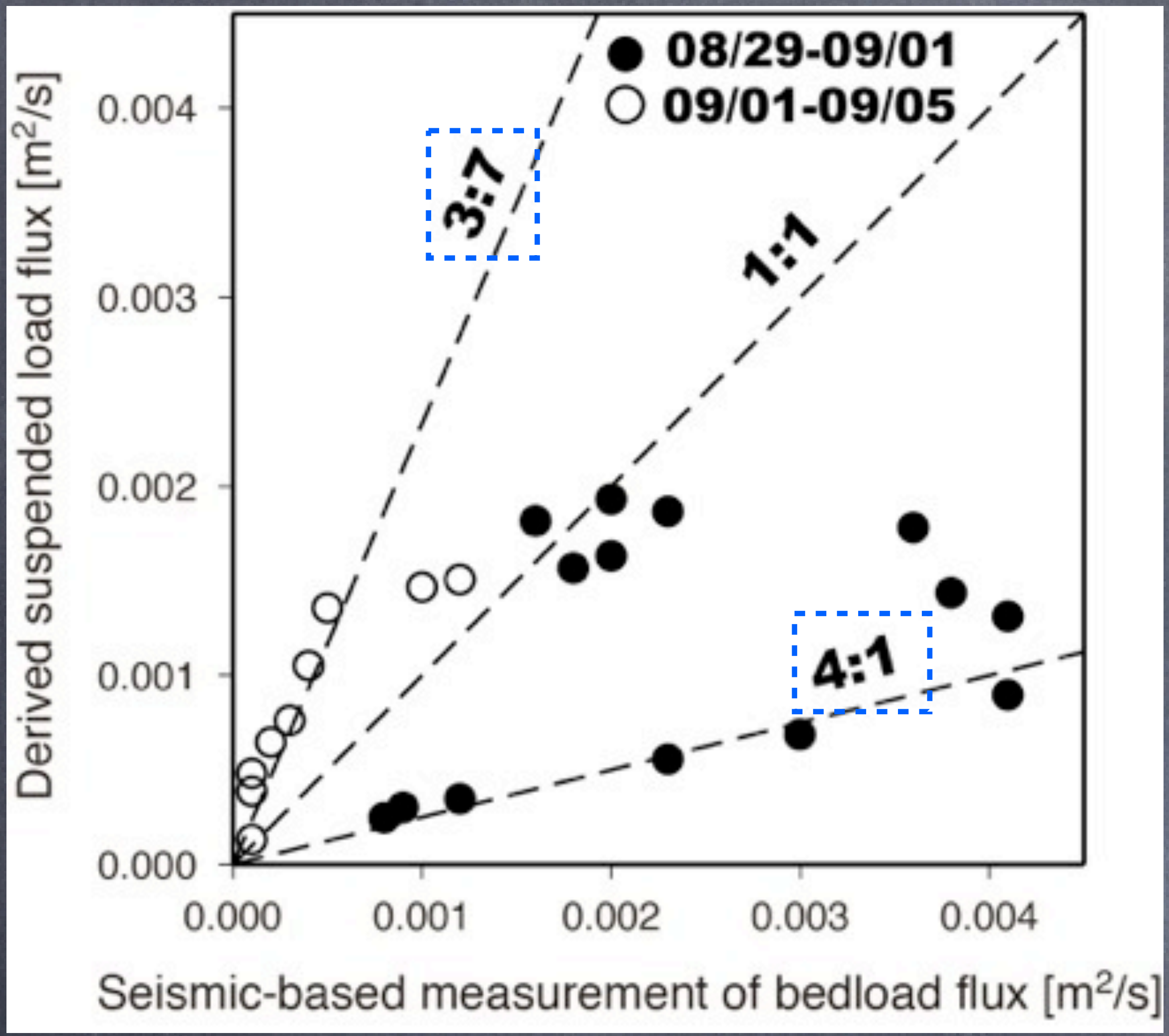

While previous studies (**repeat bathymetric surveys of water reservoirs**) found that the bedload comprises about **30 ± 28%** of the total river load in the high mountains, this fraction is likely to be temporally variable.

Our result is consistent with the ratio **3:7** during the **post-typhoon period**.

However, the bedload to suspended load sediment flux ratio roughly follows a **4:1** trend during **typhoon passage**.

In summary, the value of q_b is generally larger than q_s during the typhoon passage, and vice versa in the off-typhoon period.

Discussion & conclusions

In our results of river seismic noise analysis, the highly coherent signals in the stacked NPCCFs only appear during typhoon passage, which demonstrates the different conditions of transport capacity and sediment flux relative to the off-typhoon period.

So we conclude that the discrepancy in the scaling between q_b and q_s indicates a difference in the amount of meteorologically-controlled hillslope mass wasting into the fluvial system and/or a complex transition from the bedload regime to the suspension regime between typhoon passage and off-typhoon periods.

Discussion & conclusions

With good constraints on the grain size distribution and the seismic quality factor, our study confirms the potential of using near-river seismic noise observations (PSD) to estimate bedload flux and to further investigate the temporal changes of sediment flux ratio.

This alternative approach to bedload estimation is also useful for studying the fluvial bedrock erosion and mountain landscape evolution.

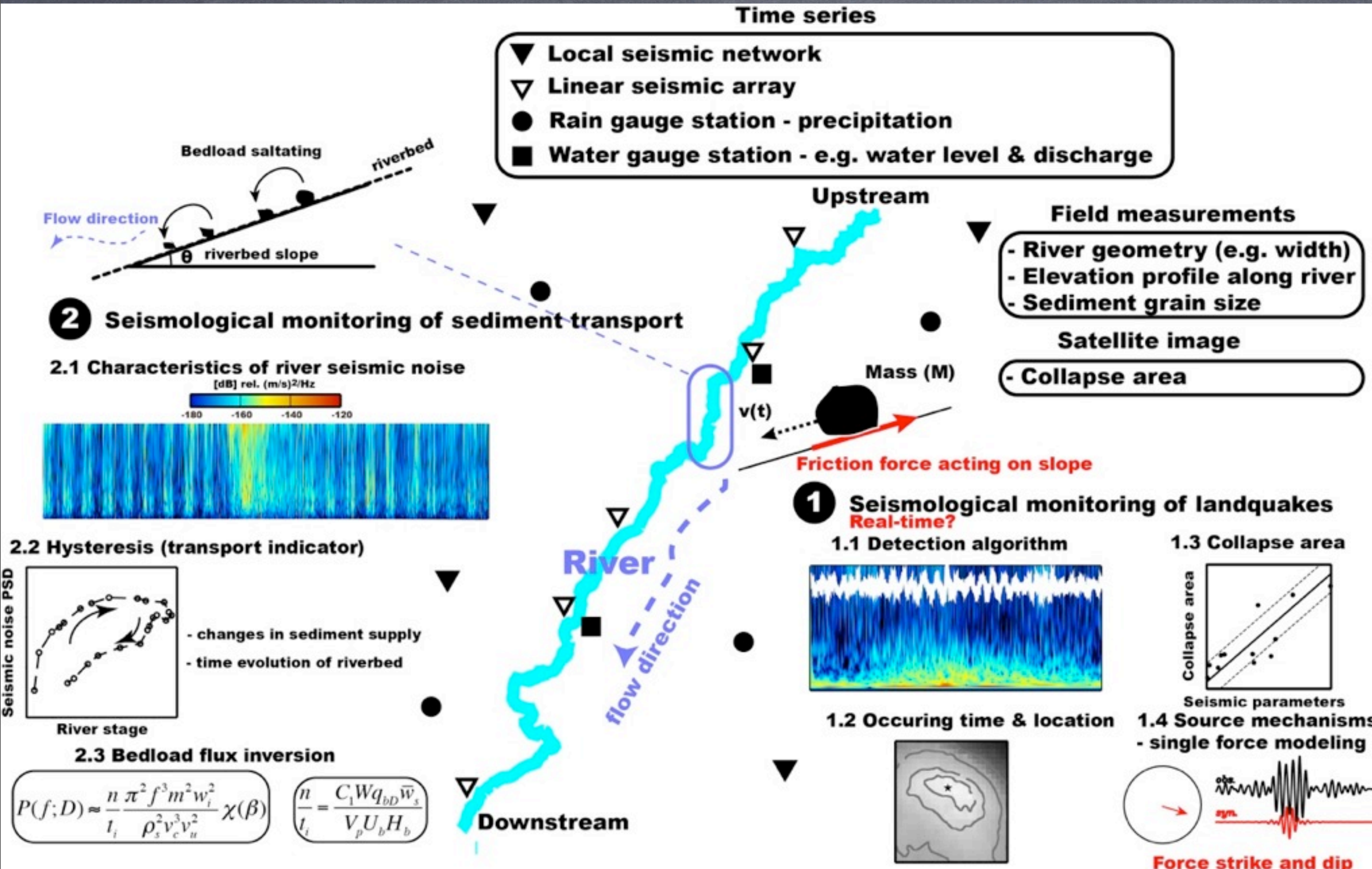

Time series
Local seismic network
Linear seismic array
Rain gauge station - precipitation
Water gauge station - e.g. water level & discharge
Bedload saltating
riverbed
Flow direction
θ riverbed slope
Upstream
Field measurements
- River geometry (e.g. width)
- Elevation profile along river
- Sediment grain size
Satellite image
- Collapse area
2 Seismological monitoring of sediment transport
2.1 Characteristics of river seismic noise
[dB] rel. (m/s)2/Hz
-180
-160
-140
-120
Mass (M)
v(t)
Friction force acting on slope
1 Seismological monitoring of landquakes
Real-time?
1.1 Detection algorithm
1.3 Collapse area
Collapse area
Seismic parameters
2.2 Hysteresis (transport indicator)
Seismic noise PSD
River stage
- changes in sediment supply
- time evolution of riverbed
River
flow direction
1.2 Occuring time & location
1.4 Source mechanisms
- single force modeling
2.3 Bedload flux inversion
$P(f;D) \approx \frac{n}{t_i} \frac{\pi^2 f^3 m^2 w_i^2}{\rho_s^2 v_c^3 v_u^2} \chi(\beta)$
$\frac{n}{t_i} = \frac{C_1 W q_{bD} \overline{w}_s}{V_p U_b H_b}$
Downstream
obs.
sym.
Force strike and dip

Field trip

Seismometers

2009-2011 ChingShui Geothermal

2010 Chenyoulan

2011 Chijiawan

Personal website: vvnchao.blogspot.tw

Mail to me: vvnchao@gmail.com

Thanks for your listening

High mountain (西巒大山)